T H E U N I V E R S I T Y O F A L B E R T A

RELEASE FORM

NAME OF AUTHOR Robert Gordon McPherson

TITLE OF THESIS A Uniformly Twisted Quadrupole Structure Produced by Point Matching of Electrostatic Potential

DEGREE FOR WHICH THESIS WAS PRESENTED Master of Science

YEAR THIS DEGREE GRANTED 1976

THE UNIVERSITY OF ALBERTA

A UNIFORMLY TWISTED QUADRUPOLE STRUCTURE PRODUCED BY POINT MATCHING OF ELECTROSTATIC POTENTIAL

by

© ROBERT GORDON MCPHERSON

A THESIS

SUBMITTED TO THE FACULTY OF GRADUATE STUDIES AND RESEARCH

IN PARTIAL FULFILMENT OF THE REQUIREMENTS FOR THE DEGREE OF

MASTER OF SCIENCE

DEPARTMENT OF ELECTRICAL ENGINEERING

EDMONTON, ALBERTA

FALL, 1976

THE UNIVERSITY OF ALBERTA

FACULTY OF GRADUATE STUDIES AND RESEARCH

The undersigned certify that they have read, and recommend to the Faculty of Graduate Studies and Research, for acceptance, a thesis entitled "A Uniformly Twisted Quadrupole Structure Produced By Point Matching of Electrostatic Potential" submitted by Robert Gordon McPherson in partial fulfilment of the requirements for the degree of Master of Science in Electrical Engineering.

ABSTRACT

The present study briefly reviews the special guiding and focusing properties of a uniformly twisted electrostatic quadrupole (helipole). A simple and unique new method for physically generating the fields of this structure is then presented and an approximate analytical solution for the fields is derived. The validity of the analysis is then examined experimentally with first a two dimensional mapping technique, and finally by constructing the structure and examining its guiding properties with the aid of a steerable electron beam which supplies a graphical output on a phosphorescent screen.

ACKNOWLEDGEMENTS

The author wishes to thank the supervisors of this project, Dr. F. E. Vermeulen and Dr. F. S. Chute, for their encouragement, and help received during the course of the study.

The able assistance of Mr. J. George in technical matters is also gratefully acknowledged.

TABLE OF CONTENTS

LIST OF FIGURES

LIST OF ILLUSTRATIONS

CHAPTER 1

INTRODUCTION

Through the years there has been an ongoing examination of many methods and structures to guide or focus streams of charged particles[1,2]. These devices cover a large spectrum of applications from the focusing of an electron beam in a cathode ray tube to the confinement of heated plasmas for fusion research. When strong transverse focusing is desired, a common structure used is the quadrupole[2,3]. The quadrupole in its most general definition consists of four electrodes (or magnetic pole pieces) arranged so as to generate transverse electric (or magnetic) fields whose intensity at any point is proportional to the transverse distance of the point from the longitudinal axis (z axis, see Figure 1). The transverse nature of the generated fields gives the quadrupole an advantage over the more classical structures where the applied field is longitudinal and hence focusing occurs only from a differential effect. Consider for example the classical structure where focusing is obtained by introducing a strong magnetic field along the longitudinal axis parallel to a stream of charged particles. The focusing force in this case is proportional to the stream's transverse velocity and is not radially directed. On the other hand in a magnetic

quadrupole the force on a particle is proportional to the stream's longitudinal velocity, which is usually higher than its transverse velocity ,and the force is radially directed. The force also increases with the radial distance of the particle from the longitudinal axis.

The quadrupole however has one inconvenient feature in that it is convergent in only one transverse direction and is divergent in the transverse direction which is perpendicular to the first one. Overall focusing can however be obtained using combinations of quadrupole structures. A brief introduction to quadrupoles and how focusing can be obtained follows in Section 1.1. Also presented is a description of a special variation of a quadrupole which is the uniformly twisted electrostatic quadrupole, or helipole. The general purpose of this thesis is to examine a unique new structure for generating the fields of a uniformly twisted electrostatic quadrupole and to then confirm the validity of the derived analysis for the structure by the construction and testing of an experimental helipole.

1.1 QUADRUPOLE LENS

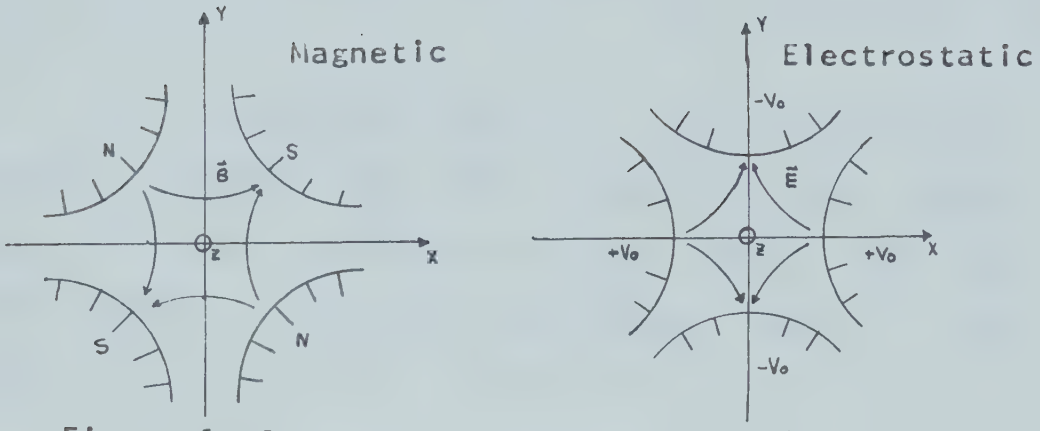

Figure 1: Cross Section of Typical Magnetic and Electrostatic Quadrupoles

A quadrupole structure consists of four hyperbolically shaped pole pieces as shown in Figure 1. The principal feature of the quadrupole structure is that the fields generated(neglecting edge effects) result in forces (F) on the charged particles which are linearly proportional to the distance of the particle from the transverse axes:

$$F_x = -q\,kX = m\frac{d^2X}{dt^2} \qquad F_y = q\,kY = m\frac{d^2Y}{dt^2} \qquad m = \frac{m_o}{\sqrt{1-\left(\frac{v_z}{c}\right)^2}} = \text{constant} \tag{1.1}$$

where k is a constant which is a function of the structure's geometry and the strength of the applied fields, q is the particles charge, and m is the relativistically corrected transverse mass of the particle.

There is thus a linear force towards one axis and a divergent force away from the other axis. The structure thus provides focusing in one transverse direction and defocusing in the other transverse direction.

Focusing along both transverse axes can be obtained by passing the particle through a series of quadrupole sections, each section being rotated through some angle relative to the previous section. The most classic combinations are the doublet, triplet and multiplet combinations[3] where two, three or more sections are used, each rotated ninety degrees relative to its predecessor.

The simplest device for obtaining focusing in both transverse planes is the doublet shown in Figure 2. The

reason for the overall focusing effect in a doublet can be seen from the following argument.

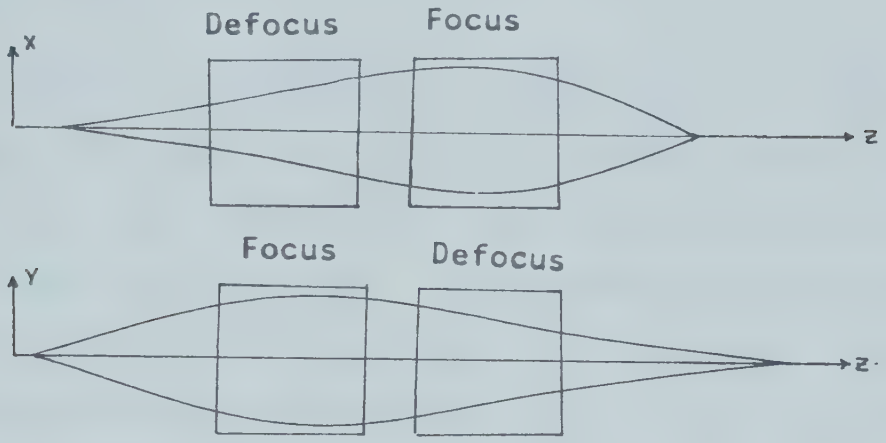

Figure 2: Quadrupole Doublet

If the first section of the doublet is defocusing, then the particles passing through the second section are further from the axis than they were in the first section. Since the restoring force is proportional to the distance from the axis, the focusing force will be larger than the defocusing force was, resulting in a net focusing effect. If, on the other hand, the first section is focusing, then the particles passing through the second section are closer to the axis and therefore are subject to defocusing forces which are smaller than the focusing forces of the first section were. This difference in forces again results in a net focusing effect.

1.2 THE HELIPOLE

1.2.1 General

A natural extension of the case of multiple quadrupole sections each rotated through some angle relative to its predecessor is to examine the limiting case of such an arrangement. The resulting structure is a standard electrostatic quadrupole with aperature radius 'a', which has been uniformly twisted β radians per metre about its Z axis, as shown in Figure 3.

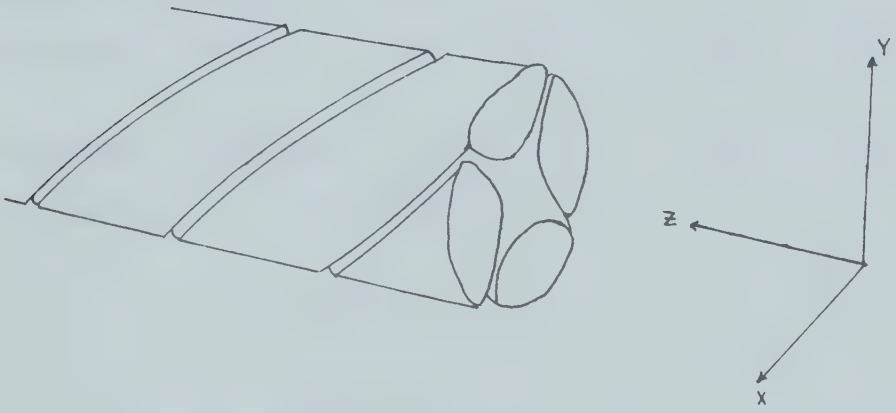

Figure 3: Uniformly Twisted Electrostatic Quadrupole or Helipole

Considerable theoretical and experimental work on the effects of such a twisted quadrupole on charged particles has been done by Youssef[4,5], Vermeulen[6], and Chute[7]. If one establishes a fixed coordinate system at the entrance plane (0) of the helipole one may describe incoming

particles in terms of their input coordinates (Xo,Yo) and actual mechanical input momenta (Pxo,Pyo) . While the particles are in the helipole their positions (x,y,z) and canonical momenta (p_x , p_y , p_z) are described in a rotating coordinate system which rotates β radians per metre with the helipole. At the exit plane (T) of the helipole a fixed coordinate system is constructed to coincide with the rotating one. Particles exiting the structure can be described in the fixed coordinate system in terms of their output position (X_T , Y_T) and output momenta (Px_T , Py_T). Since the fixed frames are chosen to correspond to the rotating ones at the entrance and exit planes of the helipole, the output coordinate plane will be rotated βz radians with respect to the coordinate input plane.

Youssef, Vermeulen, and Chute have shown that subject to the following approximations

(1.2)
$$\frac{p_x}{p_z} , \frac{p_y}{p_z} \ll 1$$
$$(\beta a)^2 \ll 1$$

an analytical expression can be derived relating the input (0) co-ordinates and momenta to the output (T) co-ordinates and momenta as follows:

$$(1.3) \qquad \begin{bmatrix} X_T \\ Y_T \\ \frac{P_{XT}}{P_{Z0}} \\ \frac{P_{YT}}{P_{Z0}} \end{bmatrix} = \left[Q(Z)\right] \begin{bmatrix} X_0 \\ Y_0 \\ \frac{P_{X0}}{P_{Z0}} \\ \frac{P_{Y0}}{P_{Z0}} \end{bmatrix}$$

$$(1.4) \qquad \left[Q(Z)\right] = \left[\begin{array}{c|c|cc} \cos\tau_1 Z & \frac{\beta\rho}{\sqrt{s-1}}\sin\tau_2 Z & \frac{\sqrt{s+1}}{\gamma}\sin\tau_1 Z & \frac{\beta\rho}{\gamma^2}\cos\tau_2 Z \\ & & -\frac{s}{\gamma\sqrt{s-1}}\sin\tau_2 Z & -\frac{\beta\rho}{\gamma^2}\cos\tau_1 Z \\ \hline -\frac{\beta\rho}{\gamma\sqrt{s+1}}\sin\tau_1 Z & \cos\tau_2 Z & \frac{\beta\rho}{\gamma^2}\cos\tau_1 Z & \frac{s}{\gamma\sqrt{s+1}}\sin\tau_1 Z \\ & & -\frac{\beta\rho}{\gamma^2}\cos\tau_2 Z & -\frac{\sqrt{s-1}}{\gamma}\sin\tau_2 Z \\ \hline -\frac{\gamma}{\sqrt{s+1}}\sin\tau_1 Z & 0 & \cos\tau_1 Z & \frac{\beta\rho}{\gamma\sqrt{s+1}}\sin\tau_1 Z \\ \hline 0 & \frac{\gamma}{\sqrt{s-1}}\sin\tau_2 Z & -\frac{\beta\rho}{\gamma\sqrt{s-1}}\sin\tau_2 Z & \cos\tau_2 Z \end{array}\right]$$

$$\gamma = \frac{1}{a}\sqrt{\frac{V_o}{V}}$$

$$\tau_1 = \gamma\sqrt{s+1}$$

$$\tau_2 = \gamma\sqrt{s-1}$$

$$s = \left(\frac{\beta\rho}{\gamma}\right)^2$$

where

$$\rho = 1 + \beta\left(X_o\frac{P_{yo}}{P_{zo}} - Y_o\frac{P_{xo}}{P_{zo}}\right)$$

P_{zo} is the Z-directed mechanical momentum at the entrance plane (the Z-directed velocity of a particle is assumed to remain constant while the particle traverses the

structure) and V is the potential through which the particle has been accelerated before injection. Vo is the magnitude of the potential at each quadrupole section and s is a stability factor whose magnitude must be greater than unity.

These results show two interesting features. First of all, the trajectories of particles through the structure are independent of their charge to mass ratios, provided that all particles have been accelerated from rest through the same potential. This result would suggest that the same helipole could guide particles ranging from electrons to micron sized charged particles of low charge to mass ratios. The second interesting property is that by choosing the length z properly, [Q(z)] becomes ±I for a given value of s, where I is the unit matrix. Hence the structure can act as a novel type of lens. In order to image a system of particles however, all of the particles must have the same stability factor 's'. An alternate expression for 's' [6] is

$$S = \frac{(\beta a)^2}{2mqV_o}\left[P_{z_o} + \beta(X_o P_{Y_o} - Y_o P_{X_o})\right]^2 \qquad (1.5)$$

All the particles of the system will then have the same

stability factor if

$$X_o P_{Y_o} - Y_o P_{x_o} = 0 \tag{1.6}$$

This result is achieved if the incoming particles can be considered as a parallel beam or as having originated from a point source.

1.2.2 Admittance and Stability Criteria

The actual paths followed by the particles, as given by (1.4), show that the distance of a particle from the axis of the lens could theoretically exceed the radius 'a' of the lens structure. Hence the particles could strike the lens electrodes for some values of input position and momenta. Therefore there are limitations on the values of input variables which can be admitted to the lens and still result in a stable trajectory, where stability means that the particle's excursions are always less than the structure's radius. It has been shown[7] that particles entering the lens must meet a confinement criterion of the form:

(1.7)

$$\left|\left[\left(X_o - \frac{\beta\rho}{\gamma^2}\frac{P_{Yo}}{P_{Zo}}\right)^2 + \frac{s+1}{\gamma^2}\left(\frac{P_{Xo}}{P_{Zo}}\right)^2\right]^{1/2}\right|$$

$$+ \left|\sqrt{\frac{s}{s-1}}\left[\left(Y_o - \frac{\beta\rho}{\gamma^2}\frac{P_{Xo}}{P_{Zo}}\right)^2 + \frac{s-1}{\gamma^2}\left(\frac{P_{Yo}}{P_{Zo}}\right)^2\right]\right| \leq a$$

CHAPTER 2

A NEW STRUCTURE

2.1 General

Electrostatic quadrupole fields are normally generated with four hyperbolic electrodes as shown in Figure 1. The potential distribution generated (neglecting edge effects) is $k(X^2-Y^2)$ where $k=Vo/b^2$. Here b is the radius of the largest circle which can be drawn on the aperature of the quadrupole without touching an electrode, and is equivalent to the aperature radius 'a' used earlier.

Considerable theoretical and experimental work has been done on the helipole structure. The structure shows particular promise of being useful in guiding and focusing particles of low charge to mass ratios. One major difficulty however, which arises because the electrodes have to conform to a helical path along the longitudinal axis, is the rather complicated fabrication and assembly procedure required to build such a structure. A possible alternative is to approximate the fields of the helipole using a much simpler structure, a task which is the major concern of the present project.

Consider the lines of constant potential for a quadrupole as shown in Figure 4. If the cylinder shown by

the dashed line were to have the potential at any given point along its surface equal to $k(X^2-Y^2)$, then the solution to Laplace's equation which meets these boundary conditions is simply the potential distribution of a quadrupole.

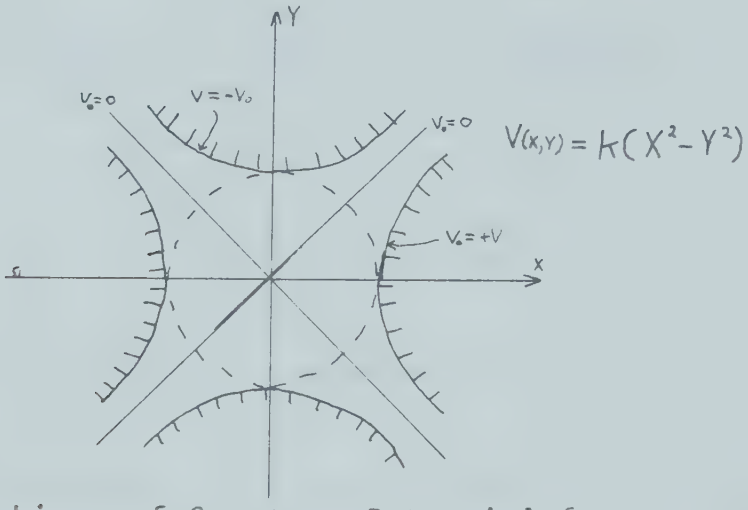

Figure 4: Lines of Constant Potential for a Quadrupole

While such continous matching of the fields to the boundary conditions is not possible, it does not seem unreasonable to assume that matching at a finite number of points may result in fields similar to those of a quadrupole.

To realize this matching, the structure depicted in Figure 5 is proposed. In this case matching is obtained at a finite number of points on the boundary, by placing thin metallic conductors symmetrically about a cylindrical surface and holding each conductor at the appropriate

potential.

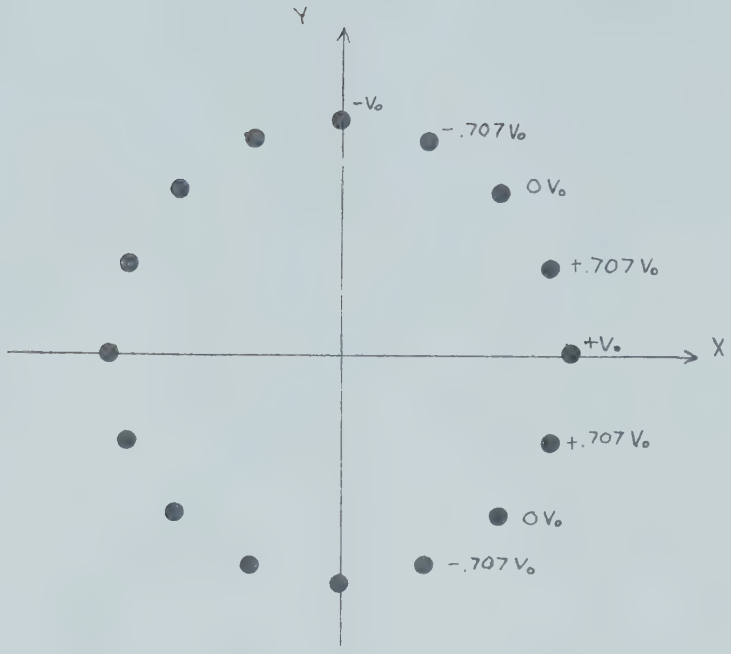

Figure 5: Potential Distribution for the New Structure

The actual fields generated by such a structure could be computed exactly by solving Laplace's equation subject to the boundary conditions presented by the conductors. However, such an analysis is impractical due to the immense complexity of the boundary conditions. For this reason an approximate analysis was developed. This analysis, which follows, yields the fields for a structure which is non-twisted. The actual solution for a twisted structure for which $(\beta a)^2 \ll 1$ can then be obtained by assuming that the aforementioned field rotates in space with the twisted structure [7].

2.2 APPROXIMATE THEORETICAL ANALYSIS

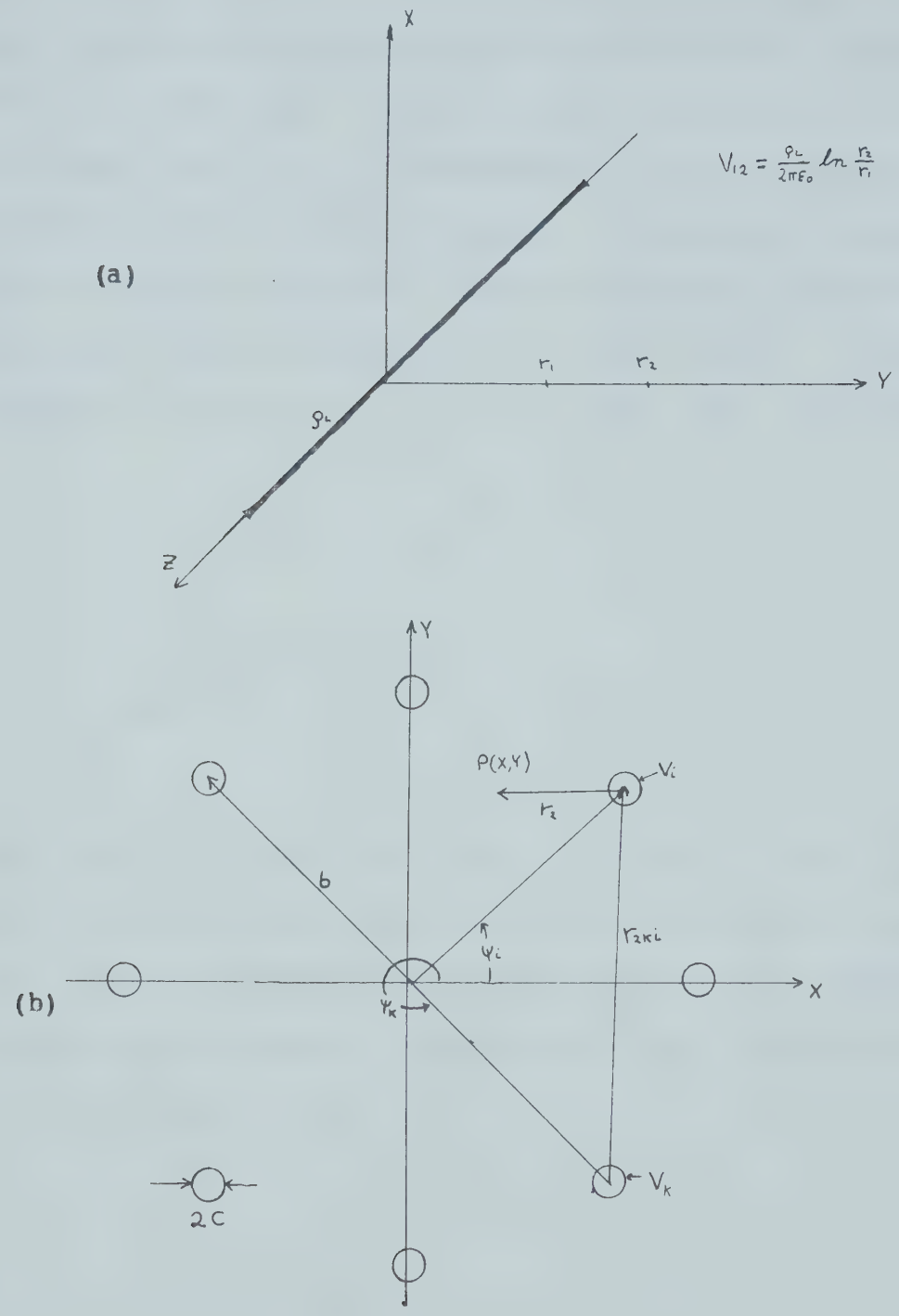

Figure 6: (a) Fields of an Infinite Line Charge
(b) Geometric Relations Between Points in the Lens

Consider the infinite line charge, of density ρ_L, shown in Figure 6(a). A uniform cylindrical conductor will have the same far fields as an infinite line charge if there is sufficient symmetry such that ρ_L will be constant along the Z axis. Therefore let us try replacing the wires by a series of line charges. Examining Figure 6(b), and defining the centre of the coordinate system as zero potential, then the potential at the point P(x,y) with respect to the origin and due to the i'th conductor is:

(2.1) $$\Delta V_{XYi} = \frac{-\rho_{Li}}{2\pi\varepsilon_o} \ln \frac{r_2}{b}$$

Then assuming, since c<<b where c is the radius of the wire, that the fields are not greatly perturbed by the fact that one has metallic conductors rather than actual line charges one can apply superposition and the total potential at P(x,y) is then

(2.2) $$V(x,y) = \sum_{i=1}^{N} \Delta V_{XYi}$$

thus giving one the potential for any point in the plane, if all of the ρ_{Li}'s are known. One cannot directly specify the ρ_{Li}'s however, one can only set the potentials on each of the conductors. One therefore computes the approximate ρ_{Li}'s by choosing them subject to the boundary condition that the potential at a radius "c" from the i'th theoretical line charge, i.e. at the surface of the i'th conductor, must be Vi. Hence from Figure 6(b)

$$(2.3) \qquad V_i \simeq \frac{\rho_{Li}}{2\pi\varepsilon_o} \ln\frac{b}{c} + \sum_{\substack{K=1 \\ K\neq i}}^{N} \frac{-\rho_{LK}}{2\pi\varepsilon_o} \ln\frac{r_{2Ki}}{b} \qquad \text{if } c \ll b$$

which can be reworked to:

$$(2.4) \qquad V_i \simeq \sum_{K=1}^{i-1} \frac{-\rho_{LK}}{2\pi\varepsilon_o} \ln\frac{r_{2Ki}}{b} + \frac{\rho_{Li}}{2\pi\varepsilon_o} \ln\frac{b}{c} + \sum_{K=i+1}^{N} \frac{-\rho_{LK}}{2\pi\varepsilon_o} \ln\frac{r_{2Ki}}{b}$$

Equation (2.4) represents N simultaneous equations which can be solved for the N ρ_{Li}'s. Hence the potential at any point in the structure can now be computed once the potential on each wire is specified. The desired potential distribution is:

(2.5) $$V(x,y) = \frac{V_o}{b^2}\left(X^2 - Y^2\right) = \frac{V_o}{b^2} R^2 \cos 2\psi$$

where ±Vo are the potentials at the electrodes of a standard quadrupole, R and ψ are the polar coordinates of the point, and b is the aperature radius. Therefore we set

(2.6) $$V_i = D V_o \cos 2\psi_i$$

where D is an arbitrary scaling factor equal to one if one wishes to match the potentials exactly.

A computer program to compute the potential distribution by this method was constructed. The results with D=1 showed that although the calculated distribution varies in the desired manner the potential is weaker in magnitude than the desired distribution. By choosing an appropriate scaling factor D however, a distribution very close to that of a quadrupole is generated (see Appendix A). Figure 7 below shows the relation between the

required scaling factor D and the number of wires used. Note that D tends toward one as the number of wires gets large. This result is consistent with the original assumption that one could generate the fields exactly if one could match the potential distribution continuously along a cylinder's surface.

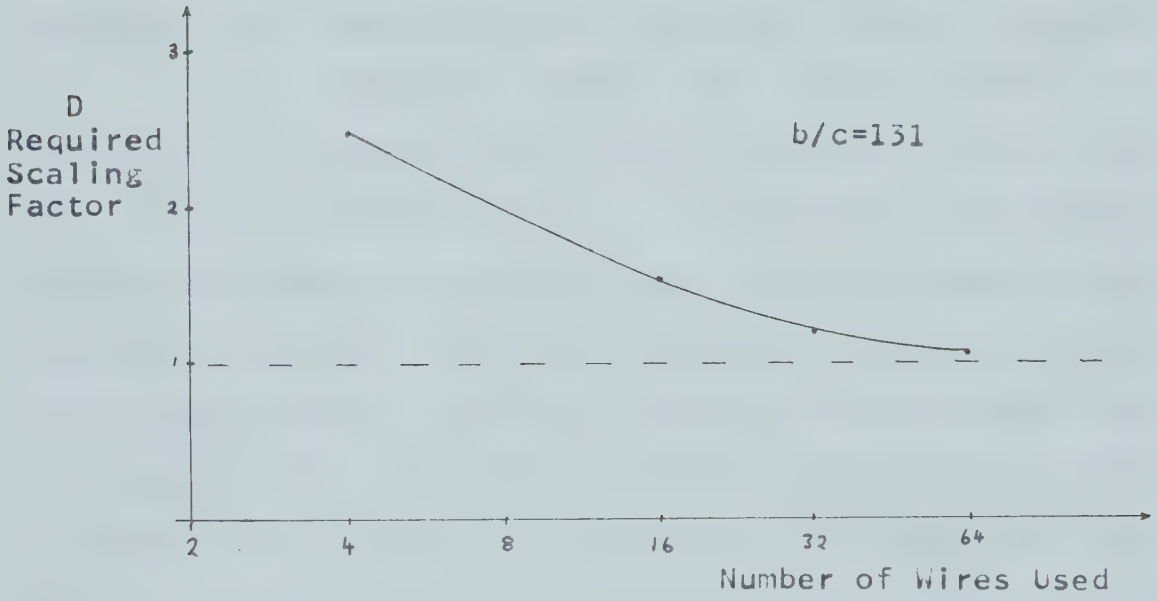

Figure 7: Required Scaling Factor Versus Number of Wires Used

CHAPTER 3

TWO DIMENSIONAL MODELING

Prior to the actual construction and testing of the proposed lens structure the author felt that some experimental evidence supporting the theoretical calculations would be appropriate. Two well known techniques exist for approximately mapping the fields of various electrode shapes. The first method[8] is to immerse a model of the electrodes in a conductive electrolytic solution, and then trace the lines of constant potential with a thin insulated probe. The second method is restricted to electrode configurations whose fields vary only over two dimensions. It consists of attaching conducting sheets of the same cross sectional shape as the desired electrode on a uniformly resistive sheet (teledeltos paper). Lines of constant potential can then be traced with a high impedance probe. The second method is considerably easier to implement and therefore was used.

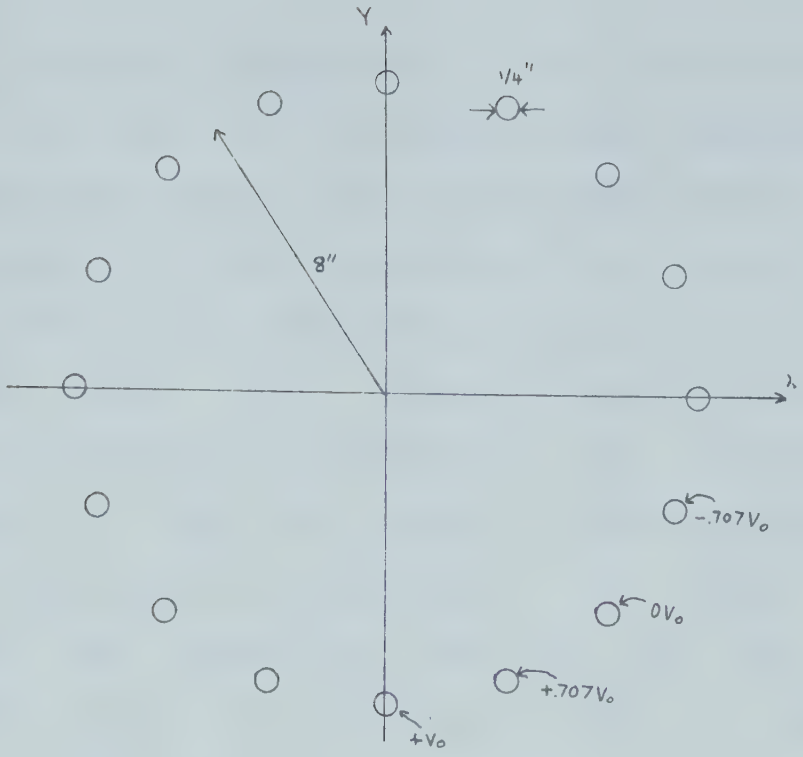

Figure 8: Diagram of Conducting Circles on Teledeltos Paper

Sixteen quarter-inch diameter conducting circles were uniformly spaced about the circumference of an eight inch circle on teledeltos paper. Each electrode was then attached with conductive epoxy and connected to the appropriate voltage as shown in Figure 8. The teledeltos paper was attached to a square cardboard backing and then inverted and supported at its four corners. A theoretical plot of $V(x,y)=(Y^2-X^2)/b^2$ equipotentials was then attached on the side of the cardboard opposite to that of the teledeltos paper (Note that in this section only, and in particular with reference to Figures 8 and 9, the

quadrupole potential distribution has been rotated through 90 degrees in the X-Y tranverse plane). Experimental points were then obtained with a split probe which had a rolling contact on the teledeltos paper side of the cardboard and a circle guide at the same position on the theoretical plot. The rolling point contact was fabricated from the tip of a ball point pen. A sample of the results is shown in Figure 9. These results were obtained using a scaling factor (D) of 1.2, which means that while the theoretical plot is for Vo=1., the experimental points were obtained with an applied electrode potential of 1.2 volts.

Using Vo=1.2 volts, a small (.02 volt) offset was found at the center which offset the experimental points slightly. However, most significant is the fact that the experimental points follow the hyperbolic shape of the theoretical constant voltage lines quite closely, indicating that the gradients of the voltage are as desired. It is the gradient rather than absolute voltage that results in the forces being proportional to the distance from the axis. This gradient is the principal feature of quadrupole fields.

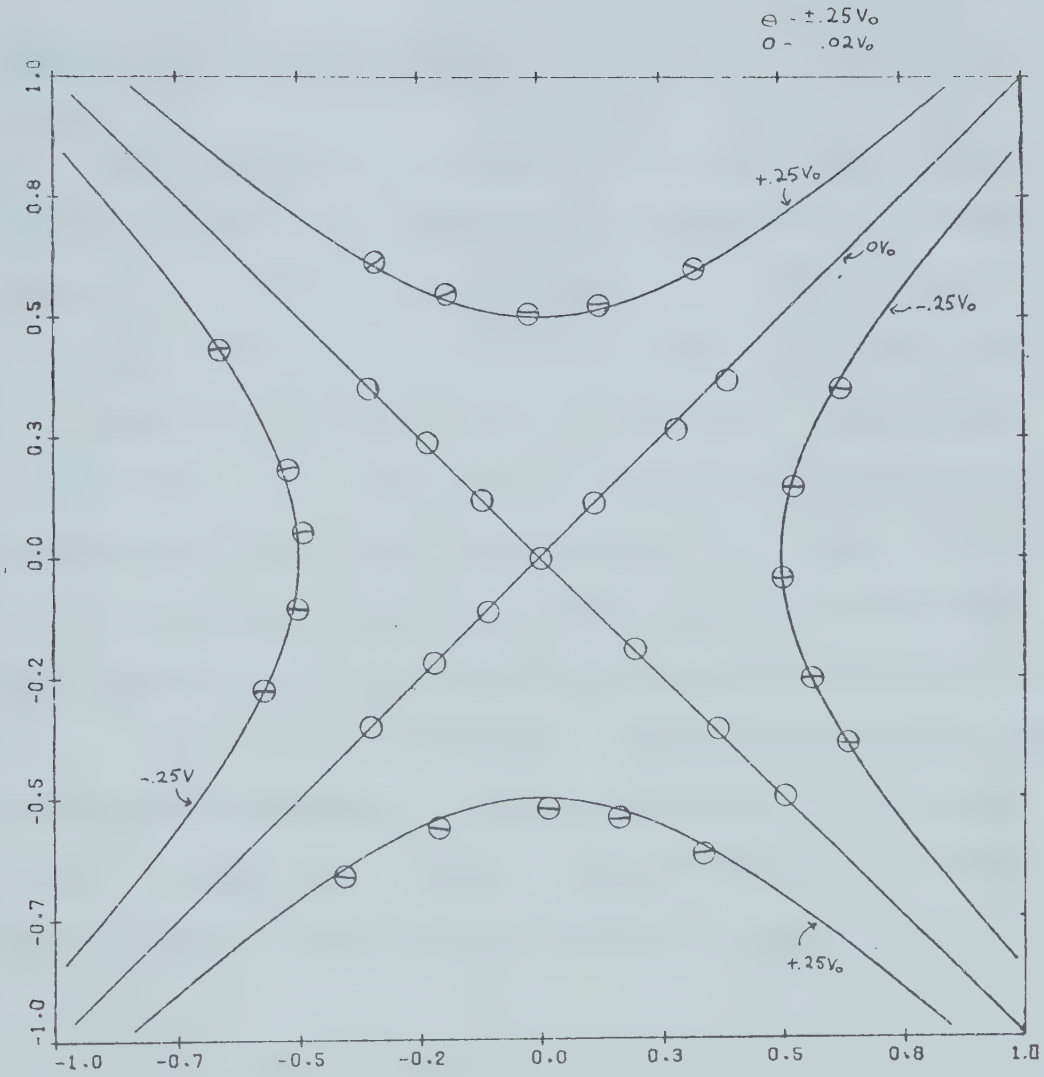

Figure 9: Theoretical Curves and Experimental Points for Two Dimensional Model as Obtained By Using Teledeltos Paper

CHAPTER 4

Experimental Investigations

As an experimental verification of the approximate analysis derived in Chapter 2, a structure to generate the electric fields of a helipole was constructed. The structure's length was carefully chosen with the intention of examining the general guiding qualities and specifically the structure's lens-like imaging properties which occur when [Q(z)] becomes ±I. In order to examine the lens' effect on charged particle trajectories the face of a cathode ray tube was cut off and the electron beam of this tube was directed through the lens onto a phosphorescent screen. It was necessary to conduct the entire experiment under high vaccum conditions. A description of the working chamber follows.

4.1 Vacuum System

The system was pumped by a Welch Model 310D turbomolecular pump(260 ℓ./sec) backed by a 8.3 ℓ./sec roughing pump and by a Varian titanium sublimation source whose speed was increased by cooling the surrounding walls with liquid nitrogen.

The working vacuum chamber itself was divided into

two parts. The quadrupole lens was mounted in a cross shaped chamber made of 6 inch diameter Corning Pyrex glass pipe. The cathode ray tube was housed in a six inch diameter aluminum pipe with electrical feedthroughs to an oscilloscope at one end and a gate valve at the other. The advantage of using a gate valve was that it allowed isolation of the cathode ray tube from the rest of the system when it was raised to air, a process that is highly detrimental to the oxide coating of the emitter of the cathode ray tube. Pressure measurements were made with a Varian NRC 531 Thermocouple Vaccuum gauge in the range 10-2000 milli-torr, and a NRC 563-P Ionization Gauge below one milli-torr.

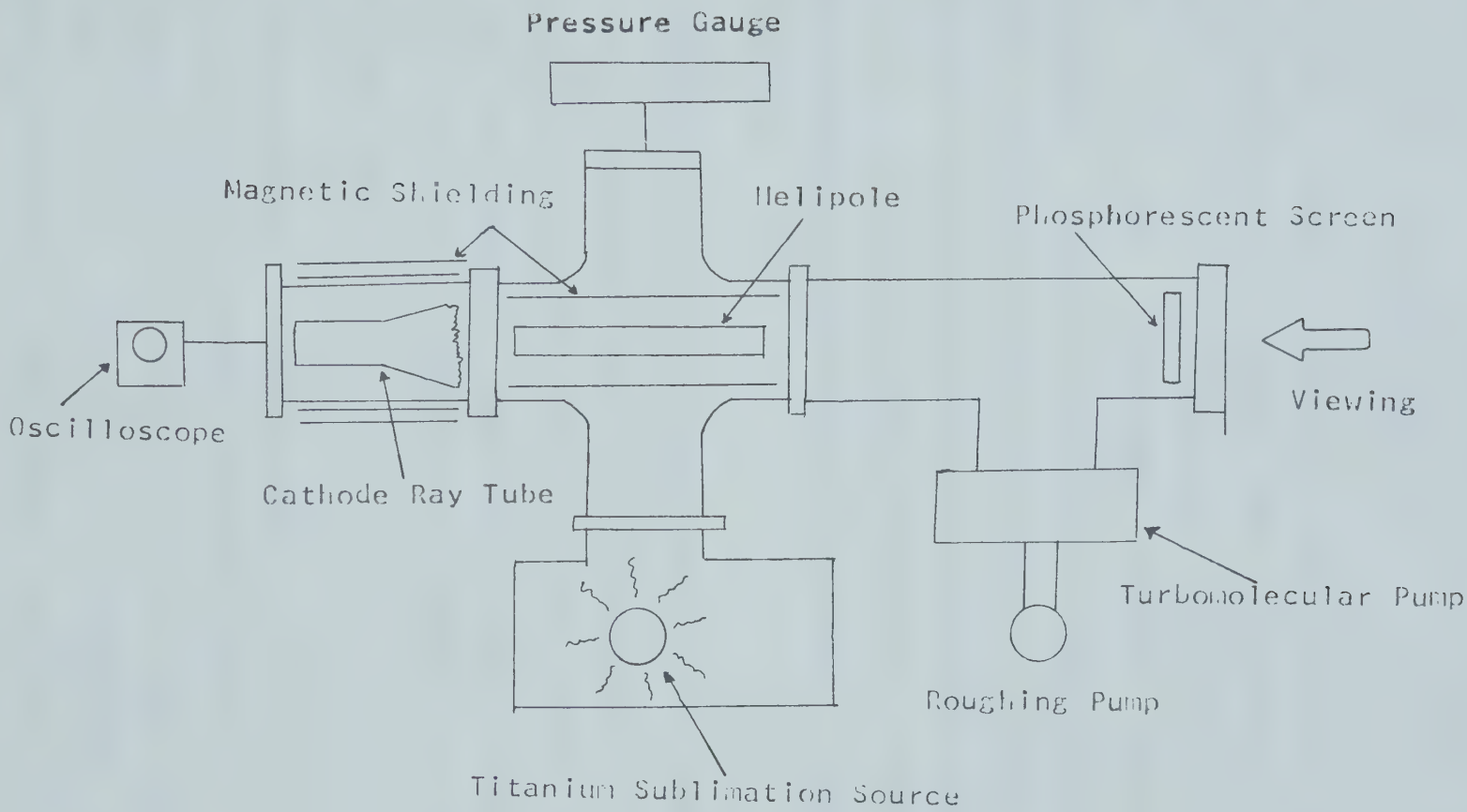

Figure 10: Vacuum System

4.2 Emitter and Detector

4.2.1 Cathode Ray Tube

Of the numerous methods of generating and detecting charged particles, the method most appealing for this project, due to its flexibility and immediate graphic output, is to use a steerable electron beam with a phosphorescent screen detector. The technology to generate, accelerate, focus and deflect an electron beam is known but is quite involved and considerably beyond the scope of the present project. Fortunately ,however, the entire technology is available in a packaged form from any oscilloscope.

The source used in the experiment is the cathode ray tube of a Tektronics type 502 oscilloscope. By removing the cathode ray tube from the scope and cutting off its face one can acquire a steerable electron beam complete with the necessary electronics package to drive and deflect the beam.

Unfortunately in the process of cutting the cathode ray tube the phosphorescent screen was damaged so that a replacement had to be built. A 6.35 mm thick glass plate was plated on one side with a transparent layer of sputtered chromium. This plate was then coated with a

phosphorous powder (Sylvania Type P161) to the density of approximately 5 mg/ cm². The chromium supplies a path for the accumulated charge to drain off as the phosphorous itself is non-conductive.

4.2.2 Spot Size

A reasonably small spot size was attainable on the face of the cathode ray tube of the oscilloscope used. However, in its final form, the path of the electron beam was lengthened by the better part of a metre. It was therefore deemed prudent to check if space charge beam spreading would be excessive.

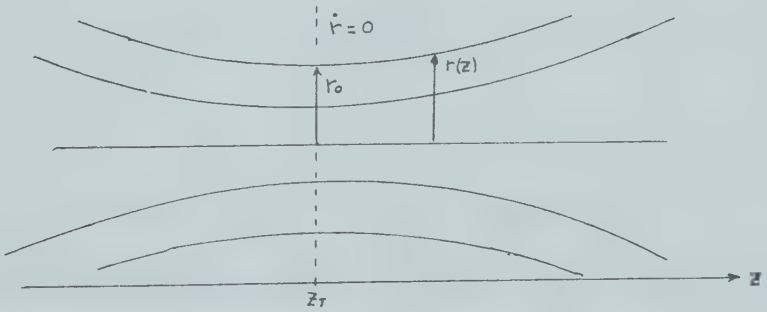

Figure 11: Rays of a Convergent Electron Beam

In any axially symmetric focusing system, a net radially inward focusing force is applied to the electron beam. In the drift space following the focusing lens the electrons drift radially inward until such time as the space charge effects become sufficient to reduce to zero

and then reverse the radial velocity of the electrons. At the point where radial velocity is zero (see Figure 11) the minimum radius r_o is obtained. By varying the magnitude of the focusing force on the beam, the target (minimum radius) plane can be shifted along the Z axis to be coincident with the phosphorescent screen.

Now let us consider the spot radius after it passes the target plane. Let us approximate it by a cylindrically symmetric, uniform density beam moving in the Z direction with zero radial velocity. This arrangement is a well known problem[9] [10] [11] and it can easily be shown that:

$$m\ddot{r}(z) = \frac{e\pi r_o^2 \rho_o}{2\pi \varepsilon_o r(z)} \tag{4.1}$$

where ρ_o is the initial charge density, r_o is the initial radius, m is the charged particle mass, r is the radius of the beam, and $\ddot{r}$ is the second derivative of r with respect to time. This equation can then be normalized and integrated numerically to generate a Universal Beam Spreading Curve (Figure 12).

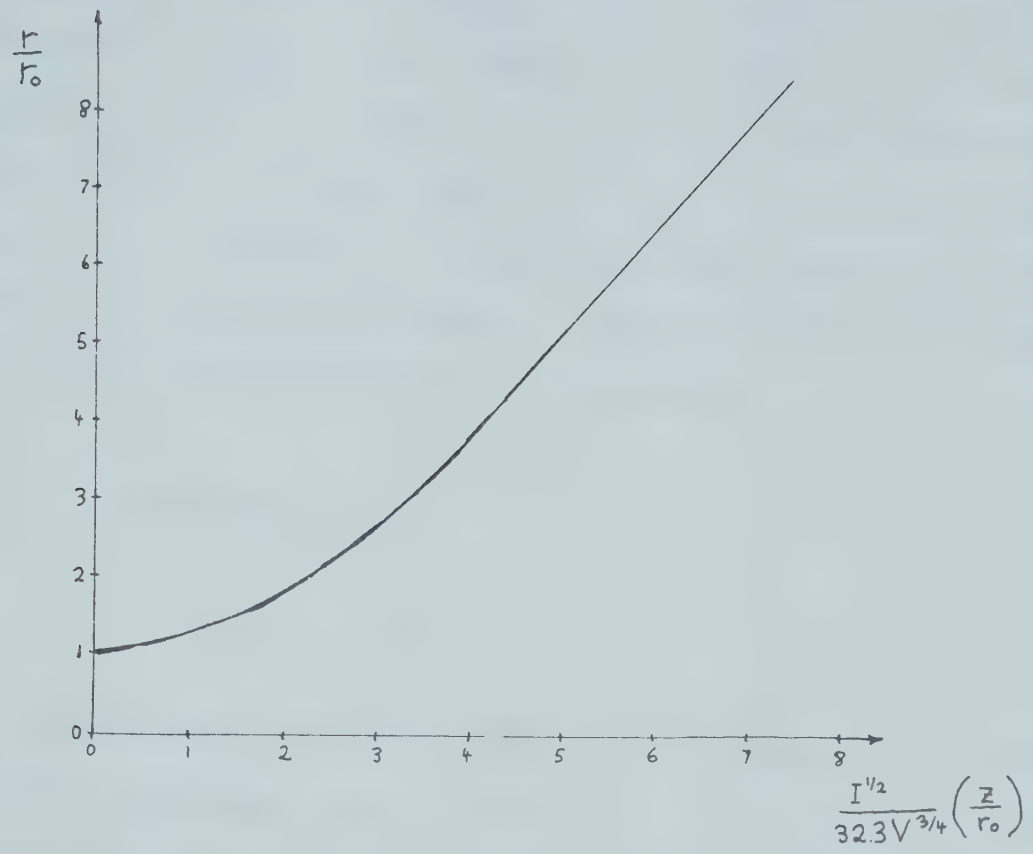

Figure 12: Universal Beam Spreading Curve

I is the total beam current in milliamperes (mA) , V is the acceleration potential (in kV) through which the beam has passed in the Z direction. For the specific case of the cathode ray tube, the potential is 3kV and the initial radius varies with the focus but is at most about one millimeter. The path length from the original cathode ray tube face to the new screen is approximately 0.8 metres. The current can be varied considerably with the intensity control but should be typically much less than one mA.

Therefore, using .1 mA, the radius will be about three times the original radius. This result is at least marginally acceptable in itself and since the analysis ignores the fact that the controls of the oscilloscope allow us to shift the target plane away from the original tube face towards the new target, beam spreading should not be an overriding problem. Experimentally a line width of one to two millimetres was obtainable.

4.3 Lens Fabrication

The lens structure nominally resembles a slowly twisted squirrel cage. Since it was desired that the individual wires be as small as possible in order to meet the approximations used in deriving the fields ($c \ll b$), a free standing structure was impossible. The lens was thus constructed by cutting slowly spiraling grooves on a cylindrical support tube into which the wires could be laid. It was hoped that by choosing a thin-walled dielectric tube with a low relative permittivity, that the support would have little effect on the fields of the helipole lens. Due to its relative availability and reasonable machining qualities , a piece of polyethylene pipe was machined to the desired specifications.

Somewhat arbitrarily, but with due consideration to the geometry of the vacuum system, a radius "b" for the twisted quadrupole of 1.66 centimetres was chosen. Then, in order to meet the approximation used in deriving the transfer matrix (equation 1.2), while keeping the helipole lens as short as possible, β was chosen such that:

(4.2) $$(\beta b)^2 = 0.1$$

This equation yields β equal to .191 radians per centimetre. The length z_1 of the helipole is nominally arbitrary. However, one of the interesting features of the transfer matrix [Q(z)] is that it becomes ±I if "s" and z_1 are chosen such that:

(4.3) $$\begin{aligned} \cos \tau_1 z_1 &= \cos \tau_2 z_1 = \pm 1 \\ \sin \tau_1 z_1 &= \sin \tau_2 z_1 = 0 \end{aligned}$$

or

$$\begin{aligned} \tau_1 z_1 &= m\pi \\ \tau_2 z_1 &= n\pi \end{aligned}$$

where m and n are integers both even or odd and z_1 is the

length of the structure. From the definition of τ_1 and τ_2 (equation 1.4) it follows that:

$$S = \frac{m^2+n^2}{m^2-n^2} \qquad (4.4)$$

Substituting for s in (1.4) and (4.3) yields:

$$Z_1 = \frac{\pi}{\beta}\left(\frac{m^2+n^2}{2}\right)^2 \qquad (4.5)$$

Obviously if one wishes to choose Z_1 with these criteria in mind then it becomes necessary to have m>n in order to keep the stability factor greater than one. Therefore in order to minimize the structure's length while still meeting the other requirements one chooses m=3 and n=1. This yields $[Q(z)]$ equal to $-I$, for s=1.25 and Z_1 =36.96 centimetres. The resulting tube was machined as shown in Figure 13.

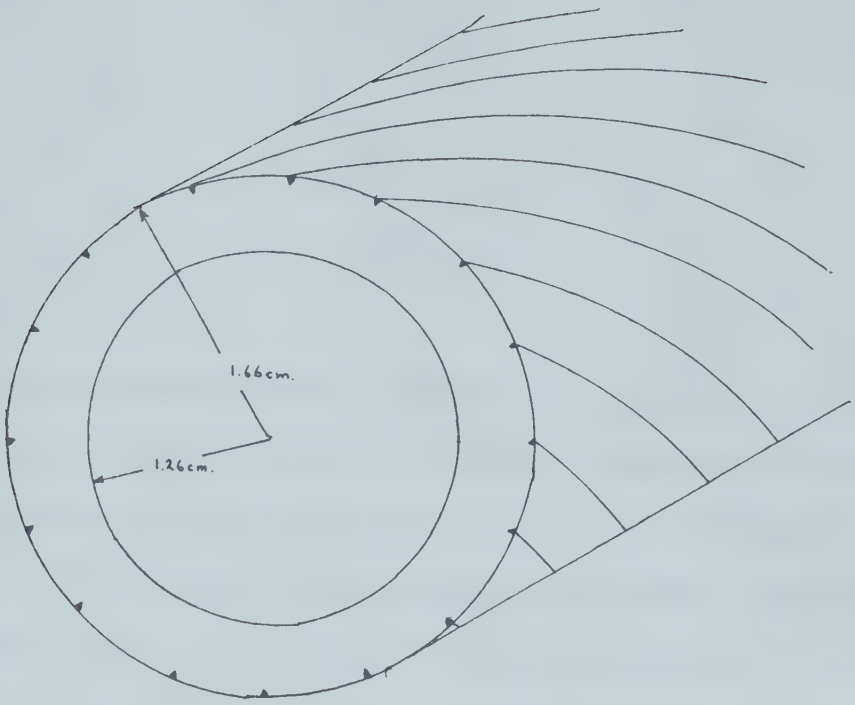

Figure 13: Helipole Support Tube

4.4 Magnetic Shielding

Since the path for the electron beam from emitter to screen was relatively large (about 1.1 metres) some difficulty was encountered due to the deflection of the beam by the earth's magnetic field.

A well known fact in magnetostatics is that a charged particle of mass m and charge q with a velocity v perpendicular to a uniform magnetic field B will describe a circular path, perpendicular to the field with radius R,

where:

(4.6) $$R = \frac{1}{B}\frac{m}{q}v$$

For the accelerating potential of the beam (3kV) and the average strength of the earth's magnetic field in the Edmonton area (5.5×10^{-5} webers/m^2) the radius is 3.36 metres. Obviously for a radius this small the beam will describe a very curved path from the source to the target. It was in fact found to be impossible to pass the beam through the polyethylene pipe used to support the lens without having the beam strike the inside surface of the tube.

It therefore became necessary to increase R significantly in order to perform the experiment. This increase can be accomplished in two ways, either by increasing the velocity of the electron beam or by reducing the ambient magnetic field. Increasing the beam velocity was ruled out due to the rather extensive modifications that would be required to the oscilloscope and cathode ray tube. Therefore, it became necessary to reduce the ambient magnetic field.

The next question then was to decide by what factor the field must be reduced. One of the more interesting properties of a helipole is that neglecting gravity, if all particles are accelerated through the same potential, then their paths are independent of each particle's particular charge to mass ratio. Being particularly interested in guiding and focusing particles of low charge to mass ratio, Youssef in his thesis[12] calculated the perturbation to the original paths due to gravity from which he derived the following inequality which must be satisfied if gravity (g) is to be neglected.

$$2\frac{gb}{\frac{q}{m}V_o}s \ll 1 \tag{4.7}$$

While it can be shown that gravity does not present any problem with an electron beam, as a first order approximation, the force on the electron due to the magnetic field could be attributed to an artificial gravity field. Thus (4.7) can be used as a standard by which one can estimate by how much the magnetic field must be reduced. One can now create the following artificial gravity (g_a):

(4.8) $$F = mg_{\star} = q v_z B = qB\sqrt{\frac{2qV}{m}}$$

Substituting in equation (4.7) yields:

(4.9) $$\frac{2B\sqrt{\frac{2qV}{m}}bs}{V_o} << 1$$

where V, Vo, q and m are as defined in section 1.2.

Substituting for the lowest value of Vo that one is likely to use (75V, for which s=4) and previously stated values for the other parameters, the left hand side of 4.9 yields a value of .927 . From this result one can ascertain that the strength of the magnetic field must be reduced by at least a factor of ten in order to satisfy the inequality.

There are three principal methods that can accomplish a reduction in fields. The first method is to rotate the experimental apparatus such that the beam path is parallel to the earth's magnetic field. In the Edmonton area however this would require rotating several tons of

equipment to an angle of about eighty degrees to the horizontal. Hence, for mechanical reasons this solution was rejected. A second alternative method would be to attempt to cancel the earth's magnetic field with an equal and opposite field generated with Helmholtz Coils. This method was eliminated due to the size of the required coils and the non-uniformities in the earth's field created by the presence of magnetic materials in and around the room, making nearly complete cancellation impossible. This result left the third alternative of using magnetic shielding. An examination of some of the literature in this field[13] [14] [15] led the author to surmise that in order to obtain the reduction in magnetic field desired (by a factor of 10 to 20), a magnetic material with a relative permeability in the order of two thousand or more was required if the shield thicknesses were to be kept reasonable. Since commercially available sheet steel only has a relative permeability of around three hundred, a slightly more exotic material was required.

A number of materials such as Mumetal, Supermalloy, and Moly-permalloy exist and are specifically made for such applications; however, their availablity and cost ruled out their use. The only material that the author was able to discover which was produced in large quantities and had good magnetic properties was the

silicon steel used in transformer cores . A small amount of 0.028 cm. thick core stock (0.011 inches) was donated by Maloney Electric Company of Canada, a transformer manufacturer in Spruce Grove, Alberta. Measurements of the final magnetic field reduction factor of the shields showed this material to have a relative permeability of approximately five thousand which was high enough to achieve the desired effects.

4.4.2 Shield Construction and Measurements

Referring to Figure 10, the geometry of the experimental apparatus was such that it was deemed necessary to construct the shield in three separate sections along the path of the electron beam. Over the area enclosed by the aluminum pipe that houses the cathode ray tube, an external two-layer shield was constructed. The inner shield for the first section was 16.5 cm. in diameter and yielded a reduction in the earth's magnetic field of approximately twelve. The outer shield was 19.1 cm. in diameter and reduced the earth's magnetic field by a factor of ten. The combination of both shields reduced the magnetic field below the threshold of the R.F.L. model 1890 Gaussmeter used, which had a zero to one gauss scale on its most sensitive setting. However, an approximate reduction factor S can be calculated from the

individual reduction factors S_1 and S_2 [14].

$$S = S_1 S_2 \left(1 - \left(\frac{d_1}{d_2}\right)^2\right) \tag{4.10}$$

This equation yields a reduction factor of forty-two.

The lens itself is housed in a cross shaped pyrex chamber, the geometry of which made an external shield impractical. Therefore a double thickness (each, .028 centimetres) cylindrical shield was constructed to fit inside the vacuum system. This shield had a diameter of 15 cm. and reduced the fields by a factor of approximately twenty-five.

With these two shields in place there was still a ten centimetre unshielded portion of the flight path in the region of the gate valve. The valve could not be operated with an internal shield in place so the external shield shown in Figure 14 was constructed.

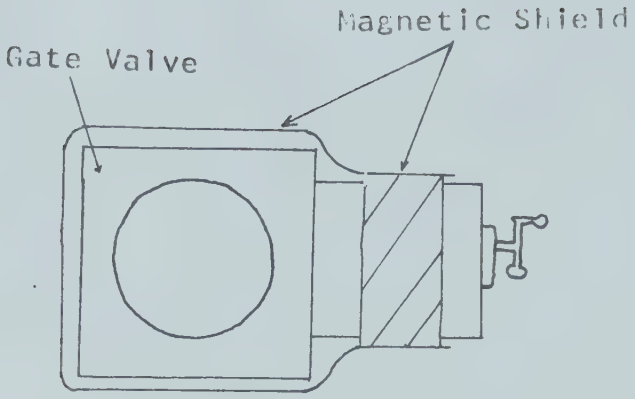

Figure 14: Gate Valve Magnetic Shield

4.5 Modifications to Analysis

4.5.1 Modifications Due To Shielding

The original analysis of the fields of the lens called for approximate matching of the fields at each of the sixteen wire surfaces. However, the addition of a cylindrical magnetic shield created an additional boundary condition to consider.

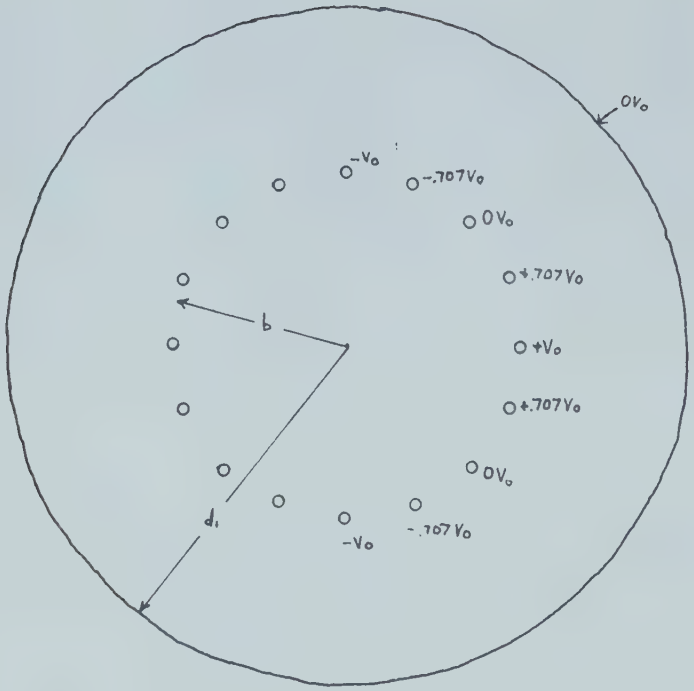

Figure 15: Boundary Conditions of Modified Structure

The original problem could only be solved by assuming that the fields of a long thin wire are the same as those of an infinite line charge. Using the same assumptions the following argument can be made.

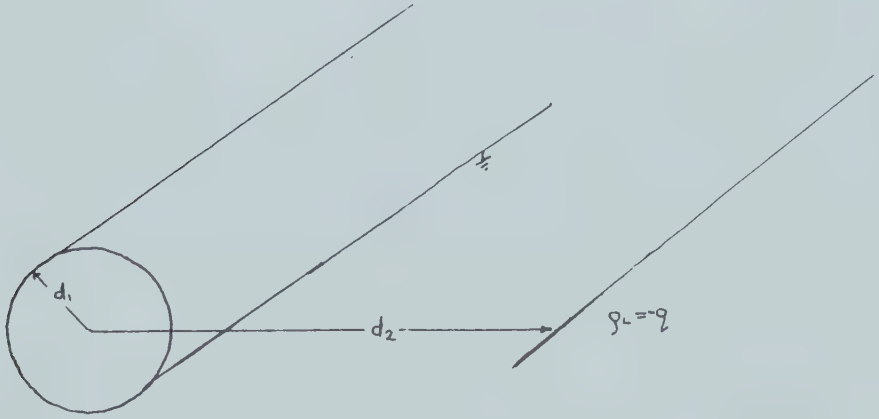

Figure 16: A Cylindrical Conductor in the Presence of an Infinite Line Charge

Considering Figure 16, one may use image theory to show[16] that the electric fields external to the conductor, due to the infinite line charge, are the same as the fields of two infinite line charges arranged in free space as in Figure 17.

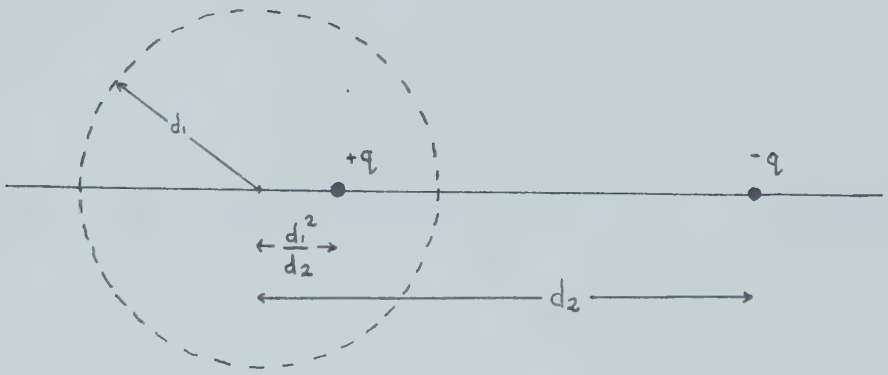

Figure 17: Equivalent Charge Distribution for the Fields External to a Cylindrical Conductor Near an Infinite Line Charge

This diagram shows how two line charges can be arranged to give an equipotential surface at a radius d_1. It further shows that since the arrangement can be rotated without disturbing the equipotential, a series of line charges can be superimposed as in Figure 18 and still maintain the equipotential surface.

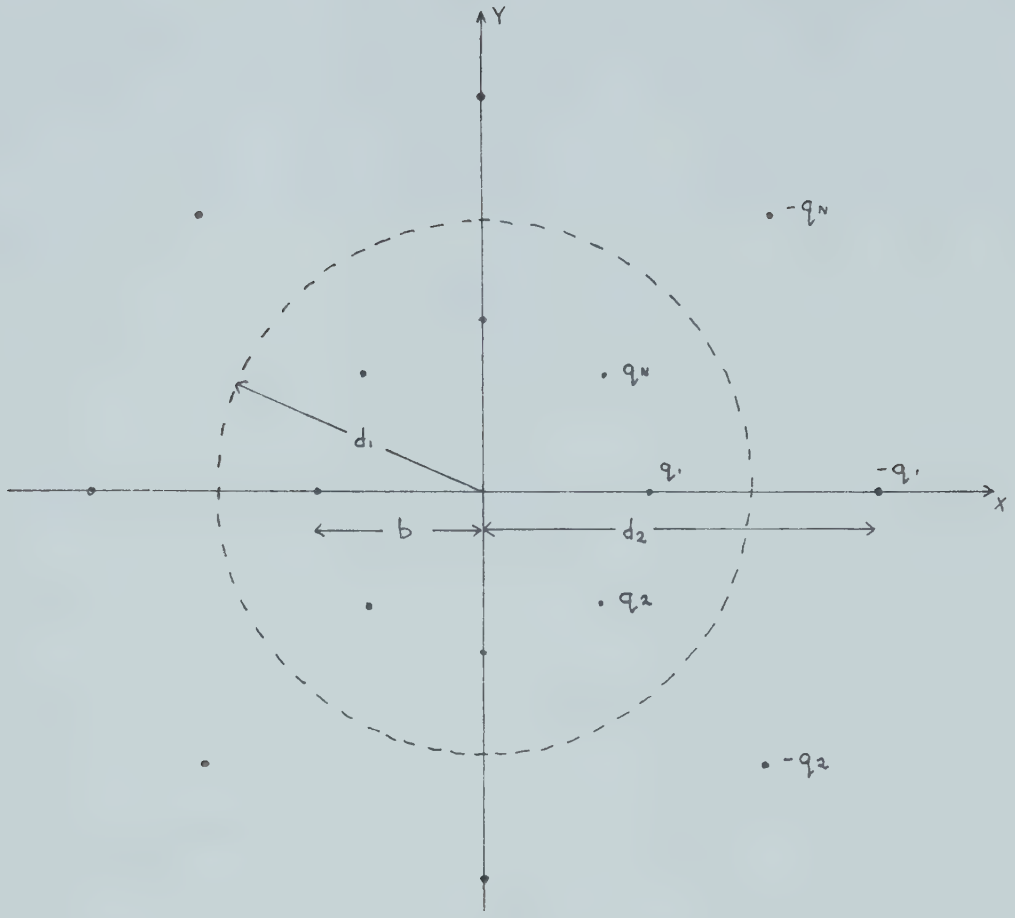

Figure 18: Superposition of Charge Distributions

It now readily follows from the foregoing exposition that the net effect of the sixteen infinite line charges at radius b surrounded by a conducting surface of radius d_1 can be predicted by removing the shield and adding sixteen image line charges at radius d_2 as shown in Figure 19.

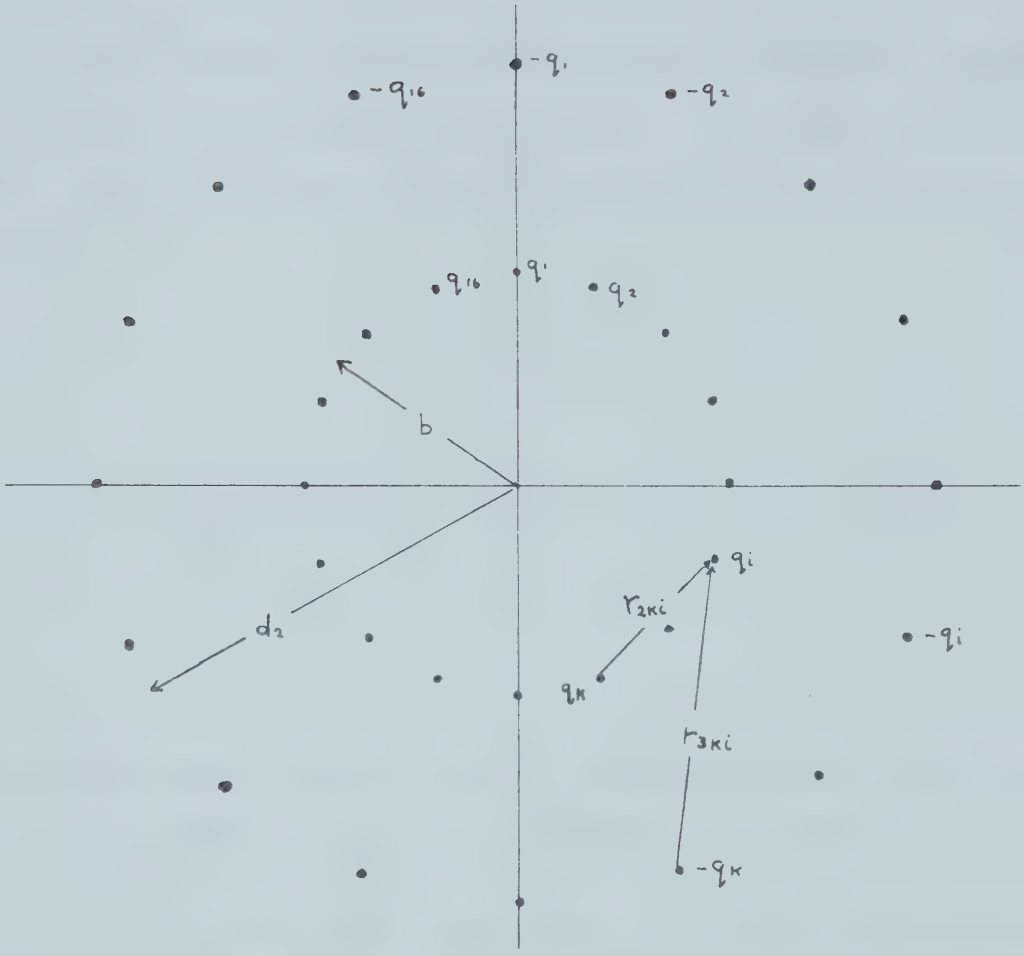

Figure 19: Equivalent Charge Distribution for a Sixteen Wire Quadrupole with a Magnetic Shield

The net effect could be considered as two concentric lenses which produce quadrupole-like fields. However, as in the original problem the charge values cannot be directly specified but must be calculated approximately from the boundary conditions. To reiterate, these boundary conditions are the potentials at the surfaces of

the wires.

If one defines the distance from the kth image charge to the centre of the ith conductor as r_{3ki} then equation (2.4) can be modified as follows to allow for the image charges.

$$(4.11) \qquad V_i = \sum_{\substack{K=1 \\ K\neq i}}^{N} \frac{-\rho_{lK}}{2\pi\varepsilon_0}\left(\ln\frac{r_{3Ki}}{b} - \ln\frac{r_{3Ki}}{d_2}\right) + \frac{\rho_{li}}{2\pi\varepsilon_0}\left(\ln\frac{b}{c} + \ln\frac{r_{3ii}}{d_2}\right)$$

This result again yields sixteen simultaneous equations which can be used to solve for the charge values.

Let us consider the values for d_1 (7.49 centimetres) and b (1.66 centimetres). Substituting these values yields that d_2 is about 22b. Calculations with and without the image charges show a difference in ρ_{li}'s of less than .1% since $d_2 >> b$. Therefore one may take the originally calculated charge values as a good approximation. Thus the potential distribution, except in the immediate area of a conductor, can be estimated by superimposing two quadrupole distributions as in equation (4.12).

(4.12) $$V(x,y) = \frac{V_o}{b^2}(X^2-Y^2) - \frac{V_o}{d_1^2}(X^2-Y^2)$$
$$= \frac{V_o}{b^2}(X^2-Y^2)\left(1-\frac{1}{22^2}\right) = .998\frac{V_o}{b^2}(X^2-Y^2)$$

It therefore follows that the shield radius in this particular case is sufficiently large that the effect on the fields is negligible.

4.5.2 Modifications Due to the Dielectric Support Tube

The polyethylene tube used to support the lens structure has a relatively low dielectric constant (relative permittivity of 2.25) and was made as thin as possible to minimize any changes to the electric fields of the helipole.

An approximate calculation of the perburbation to the electric fields due to the dielectric tube can be performed as follows. In the original derivation it was shown that the sixteen wires generated electric fields similar to those of a cylinder with the potential distribution $K(X^2-Y^2)$ at any point along it's surface. Consider, therefore, the two dielectric boundary value problem as presented in Figure 20.

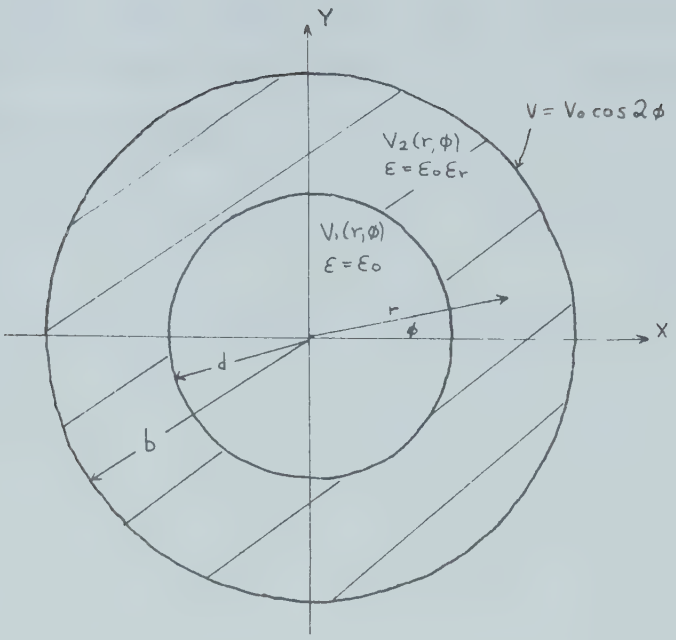

Figure 20: Boundary Value Problem of the Dielectric Support Tube

A general solution to Laplace's equation in cylindrical coordinates with no longitudinal variations[17] is:

$$(4.13)\quad V(r,\phi) = \left(B_1 r^n + B_2 r^{-n}\right)\left(B_3 \cos n\phi + B_4 \sin n\phi\right)$$

This equation is the general form of the solution assumed for $V_1(r,\phi)$ and $V_2(r,\phi)$, the potential distributions for the air and dielectric regions respectively. The constants were then evaluated by using the boundary condition for

potential at r=b and r=0, and the required boundary conditions on the electric field at r=d. This derivation (see appendix B) yielded:

$$(4.14) \qquad V_1(r,\phi) = C\,\frac{V_0}{b^2}\,r^2\cos 2\phi = C\,\frac{V_0}{b^2}(X^2-Y^2)$$

where

$$(4.15) \qquad C = \frac{b^4}{d^4}\left[\frac{\left(\frac{\varepsilon_r+1}{\varepsilon_r-1}\right)\left(1-\frac{b^4}{d^4}\right)}{\left(1+\left(\frac{\varepsilon_r+1}{\varepsilon_r-1}\right)\frac{b^4}{d^4}\right)} + 1\right]$$

The constant C reduces to one as d approaches b or as ε_r approaches one, thus yielding our original solution for quadrupole fields. However for ε_r equal 2.25 and d equal .76b, as shown in Figure 13, the value for C is 1.23, indicating that the electric fields will be approximately twenty-three per cent stronger due to the support tube. This result would imply that the required scaling factor D must be reduced by a similar factor.

4.6 Experimental Results

4.6.1 Specific Admittance Limits

The source of the electron beam is a narrow angle cathode ray tube so that, to a very good approximation any electron entering the lens from the gun can be considered as originating from a point source at the deflection plates of the gun. For a point source the stability factor (eqn. 1.4) becomes:

$$S = (\beta b)^2 \frac{V}{V_o} = \frac{300}{V_o} \qquad (4.16)$$

Since the stability factor must be greater than one, the upper limit for the quadrupole voltage (Vo) will be three hundred volts. A lower limit of 75V was established in section 4.4.1 due to the earth's magnetic field. However, since the magnetic shielding after construction yielded a larger reduction in field than was first calculated as a minimum, this limit can be lowered somewhat.

With a point source, the input momenta will be tied to the input position and thus the confinement criteria (1.7) presented in section 1.1.2 can be reduced to the two input position variables. Specifically:

$$\frac{P_{xo}}{P_{zo}} = \frac{X_o}{w} \qquad \frac{P_{yo}}{P_{zo}} = \frac{Y_o}{w} \tag{4.17}$$

where w=57.2 cm is the distance from the gun deflection plates to the helipole entrance plane. Substituting .76b for 'a' in equation (1.7) in order to account for the reduction of the usable aperature due to the dielectric support tube of the lens, and substitution of equation (4.17) yields an irreducible equation in Xo and Yo. The equation however can be solved numerically to show the portions of the entrance plane which can be used. The acceptance regions for various values of quadrupole voltage are shown in Figure 21.

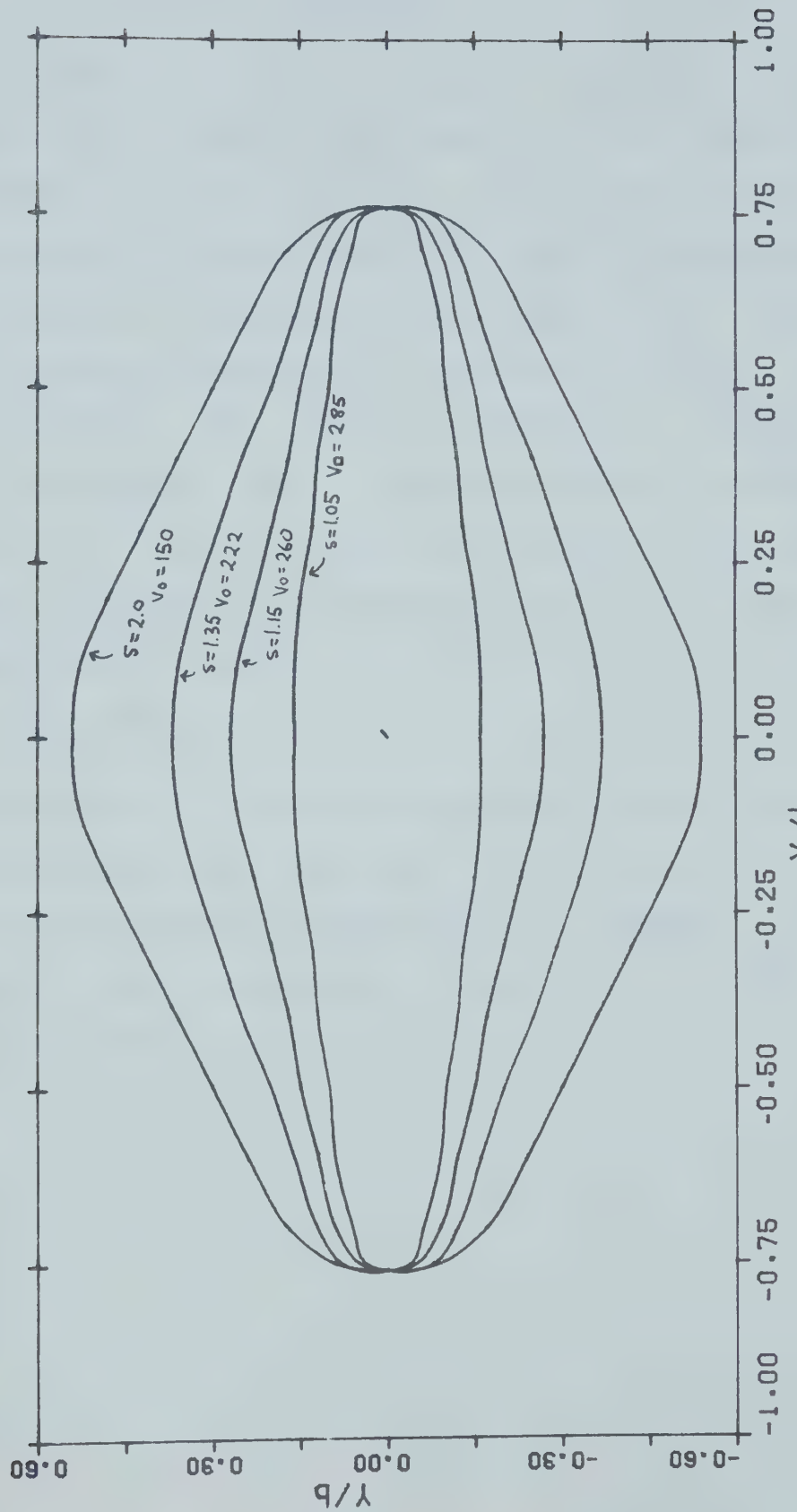

Figure 21: Specific Admittance Regions for Experimental Helipole Lens

4.6.2 Horizontal Line Rotations

An examination of the specific admittance limits derived in the previous section shows that any figure that one desires to describe with the electron beam on the entrance plane of the helipole, must have a rather small Y axis component if one desires to use most of the allowable range in quadrupole voltages. Therefore the first figure used to examine the guiding properties of the lens is simply a horizontal line. A computer program to calculate the path of a point source derived horizontal line through the lens and across the drift space from the exit plane to the phosphorescent screen was developed using the transfer matrix [Q(z)] (eqn. 1.4).

Theoretically a straight horizontal line will undergo a simple rotation, the angle of which varies with the quadrupole voltage but is independent of the line's radial amplitude. The theoretical output for a number of voltages is shown in Figure 22.

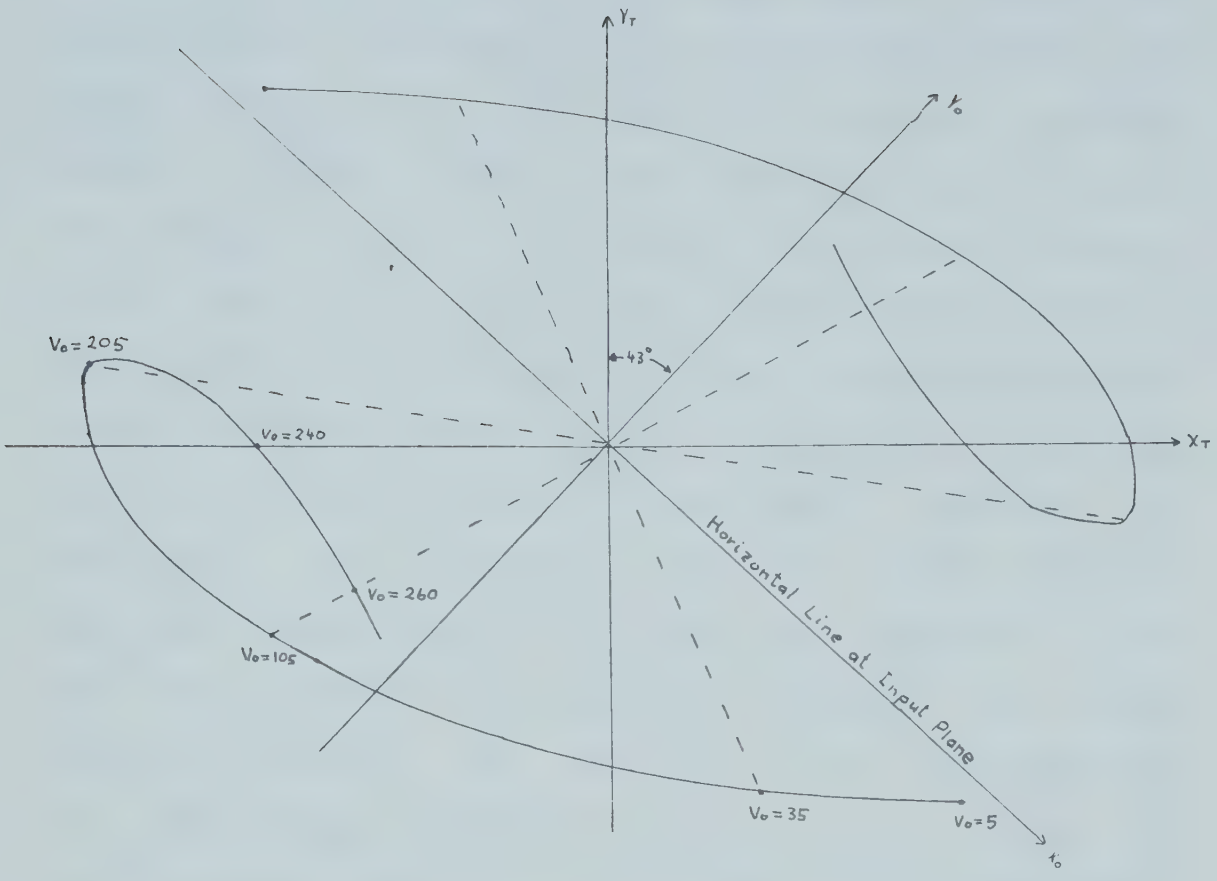

Figure 22: Horizontal Line Rotations with Electrode Potential

The dashed lines represent the output for various values of voltage and the solid lines represent the track of the end points of the horizontal line with voltage.

There is thus a functional relationship between rotational angle and lens voltage. This theoretical curve is presented in Figure 23 along with several

experimentally measured points which were obtained by photographing the output of the phosphorescent screen for various values of Vo. Note that these points are plotted using a scaled voltage rather than the actual voltage. The voltage values corresponding to the experimental points have been divided by a scaling factor of 1.29. This value of scaling factor was found to be approximately optimal for the present geometry (see section 4.6.3). The theoretical scaling factor for the specific geometry of the system was calculated to be 1.55. Recall, however that the electric fields of the lens were computed to be 1.23 times stronger than originally calculated, due to the dielectric support tube (section 4.5.2). Therefore the net theoretically required scaling factor would be 1.55/1.23=1.26 which is quite close to the experimental value obtained.

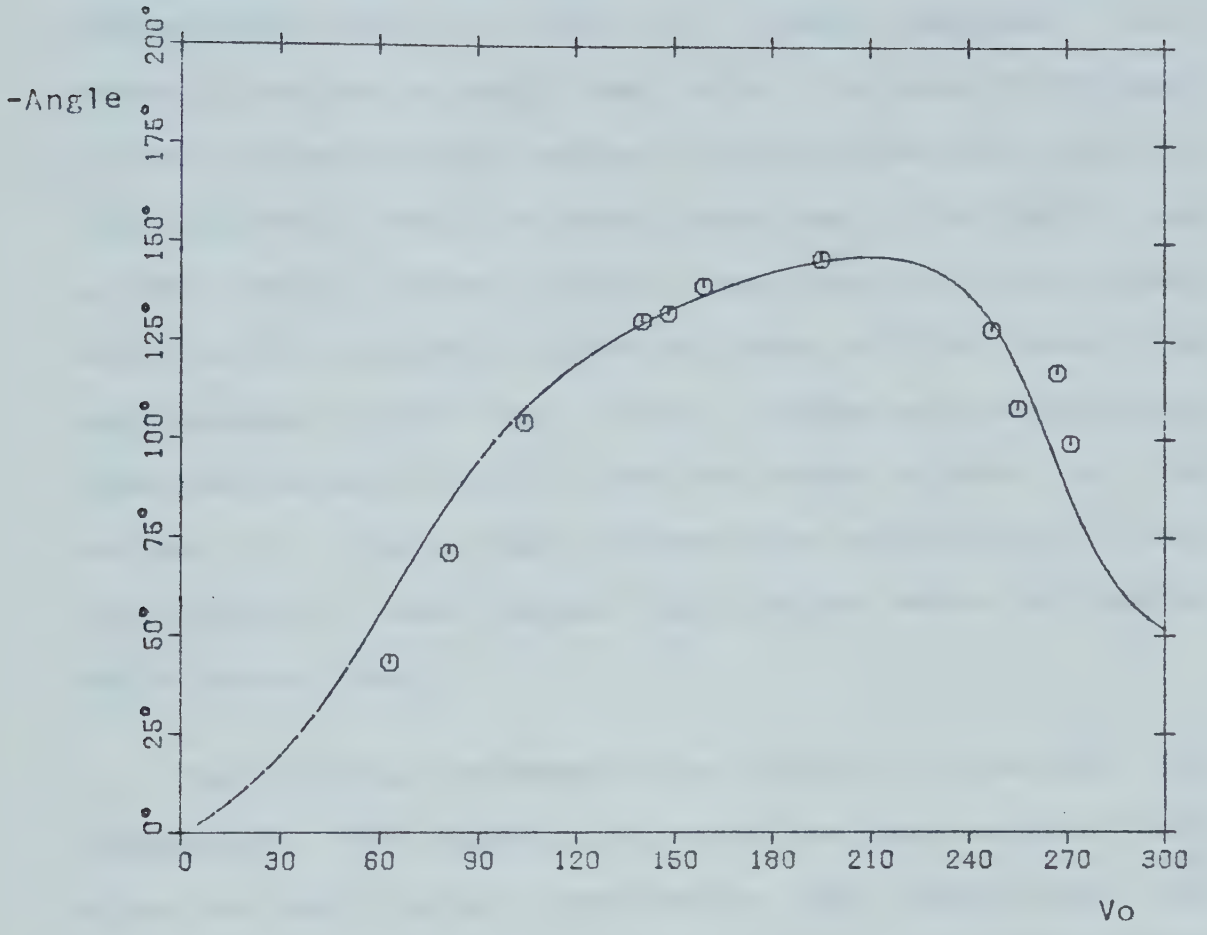

Figure 23: Rotational Angle Versus Electrode Potential

A number of difficulties arose while taking these measurements which necessitated rejecting a number of the photographs. The most difficult problem to overcome was charge build-up on the support tube of the lens. If at any point in the process of setting up and measuring the line rotations, the beam was allowed to strike the

polyethylene tube then, since the tube was an insulator, a charge would build up along its inside surface. This charge distribution would then affect the path of the beam in an unpredictable manner for some time (up to two or three minutes) until it would bleed away. Initially one of the major causes of this charge build-up was thermal drift in the deflection plate voltages as the tube type oscilloscope warmed up. This problem was rectified by inserting an extra switch into the heater circuit of the cathode ray tube which allowed the oscilloscope to run long enough to reach thermal equilibrium before activating the electron beam.

The following procedure was used to minimize the probability of charge build up on the lens support tube. After the oscilloscope electronics had stabilized, the spot of the cathode ray tube was displayed. If the spot was not centered it would describe an arc similar to that shown for the end points of the horizontal lines (as shown in Figure 22) when the lens voltage was increased and decreased. By adjusting the horizontal and vertical offset controls of the oscilloscope the arc could be reduced to just a rotation of the spot. The beam was thus centered. The desired lens voltage was then applied and the beam expanded into a line sufficiently large to photograph reasonably well. The voltage was then reduced to zero. If no charge build-up had occurred, then the

line would immediately return to a horizontal position. If charge build-up had occurred, then the line would generally maintain some angle to the horizontal and slowly drift back to a horizontal line. The photograph would in this case be rejected. This phenomenon was found to occur most prevalently in the two to three hundred volt range where allowable acceptance regions made measurements (particularly those approaching 300 volts) difficult to obtain (see Figure 21).

Another difficulty emerged part way through the measurements. Quite unexpectedly the spot displayed split into two separate spots. Initially it was assumed that some type of electrical interference was possibly being coupled into the system. Thus the layout and shielding of some of the feeds to the cathode ray tube were modified and the effort was rewarded by the number of the spots increasing from two to three and then to four. Feeling that such a complex wave form was unlikely from electrical interference an alternate source of this phenomenon was sought. If not deflected by fields, the beam position could be changed by physically moving the cathode ray tube. It was postulated, therefore, that the cathode ray tube and its supports were rocking in some complex forced oscillations fed by vibrations through the structure originating from the turbo-molecular pump. The somewhat pragmatic approach of sharply tapping the experimental

chamber with a hard object temporarily squelched the oscillations.

A few of the actual photographs obtained are presented in Illustration 1. The actual unscaled electrode voltage is supplied with each photograph. Note that in the Vo=133V case a small mechanical vibration is superimposed on the electrostatic plate deflection, causing the line to spread and almost form two close parallel lines. The relative angle measurements for the experimental points shown in Figure 23 were obtained by measuring the angle between the line in the Vo=0 photograph and the lines in the other photographs. It should be pointed out that in view of all the aforementioned experimental difficulties approximately two weeks were required to compile the eleven experimental values shown in Figure 23. While no quantitative error analysis was attempted the agreement with the theoretically expected curve lends a measure of confidence to the experimental values. Note that it is to be expected that the agreement between theory and experiment will be less precise at high and low voltages. At high voltages the angular rotation per volt is large and small errors in quadrupole voltage can produce anomalous line rotations. At low quadrupole voltages the residual magnetic field can significantly perturb the particle trajectories.

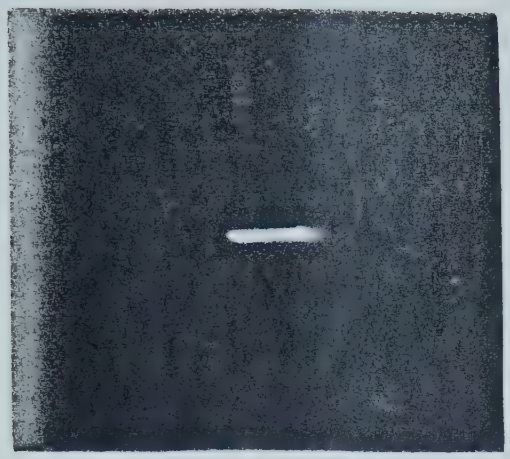

0. Volts

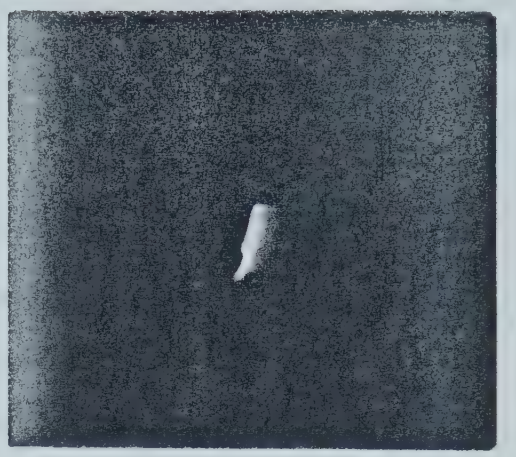

133. Volts

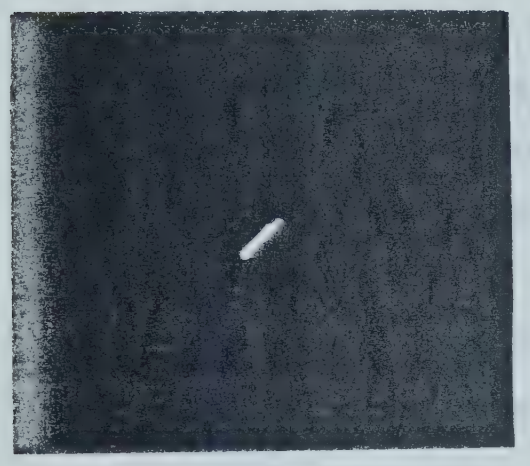

184. Volts

329. Volts

ILLUSTRATION . 1 .

LINE ROTATIONS .

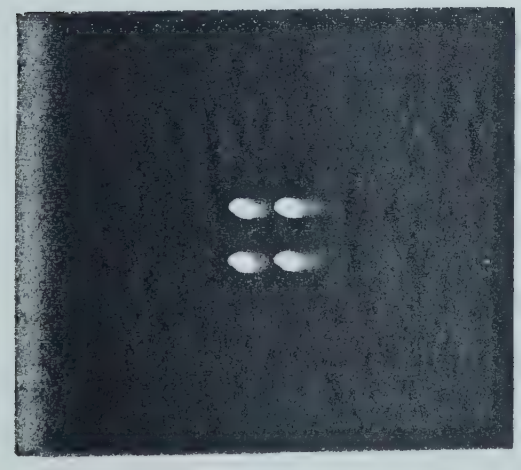

0. Volts

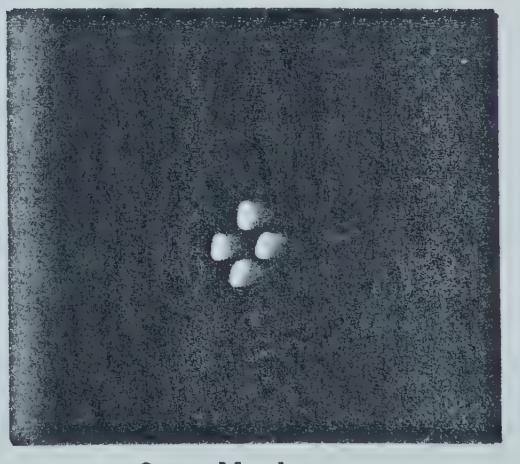

207. Volts

ILLUSTRATION. 2.

HELIPOLE EFFECTS ON RECTANGLES

4.6.3 Other Figures

It was felt that the effect of the helipole on some figures more complex than a simple horizontal line would provide a more graphic illustration of the effects of the helipole. Specifically, the unique property of imaging the input positions and momenta for a specific value of lens voltage (240 V) was of interest. However from the admittance curves (figure 21) it can be seen that the acceptance area shrinks rather rapidly in the 200 to 300 volt range. Experimentally it was found that the charging of the lens support tube was difficult to avoid if figures much larger than the obtainable line width were attempted. For this reason values more in the mid-range of allowable lens voltages were used.

Accurate amplitude measurements of the size of a figure were difficult due to the relatively large size and irregular shape of the spot obtained at the target. However, as in the case of the horizontal lines, reasonably accurate relative angle measurements between lines could be made. Therefore, the second figure chosen was a rectangle. However, rather than generating an actual rectangle it was found to be easier to simply generate a spot at each corner of the figure, as shown in Illustration 2. The required voltage waveform necessary

to generate this figure is quite easily obtained by attaching two J-K flip flops in series to form a binary counter. The output of the counter, when driven with a master clock, has four distinct states (one for each corner) and can be applied to the horizontal and vertical deflection plates of the cathode ray tube in order to generate the desired figure.

The form of the rectangle for the values of electrode voltages of Vo=0 and Vo=207 volts is shown in Illustration 2. By substituting the input positions and momenta of the new figure into the computer program developed for the horizontal line rotations, the output for various values of Vo can be computed. Theoretical outputs, similar to those of Illustration 2, are shown in Figure 24 for several values of Vo.

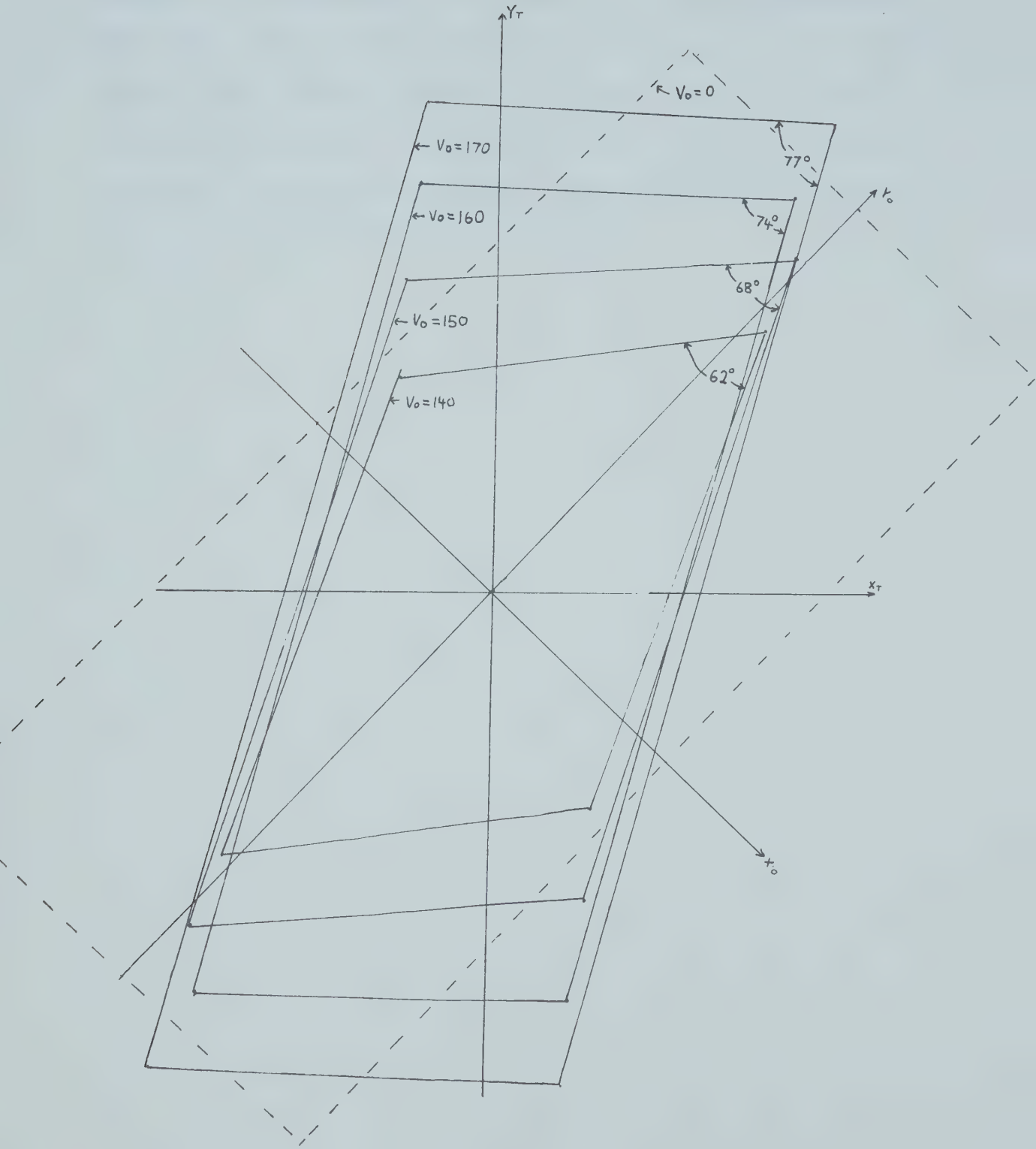

Figure 24: Helipole Effect on a Rectangle for Various Values of Vo

For Illustration 2 the measured value of the included angle, as indicated in Figure 24, is approximately 75 degrees. This angle implies a lens voltage of Vo=160V. Since the actual helipole voltage used was 207V, the indicated scaling factor is 1.29. This experimental scaling factor agrees almost exactly with the theoretical net required scaling factor of 1.27.

CONCLUSIONS

A new structure to generate the uniformly twisted quadrupole fields of a helipole has been proposed. An approximate analytical solution for the quadrupole fields has been derived and has been verified by both a field mapping technique and by constructing an experimental helipole. Some basic guiding properties of the helipole were demonstrated with the aid of a steerable electron beam. Close agreement was obtained between the analytical solution and the experimental results. The helipole developed in this thesis is much more easily constructed than a conventional quadrupole system. It should be relatively simple to construct a helipole guiding system by twisting the appropriate electrode wires about an insulating tube, reversing the pitch as necessary to produce any desired quadrupole multiplet effect.

Alignment problems, which are common to standard quadrupole systems, are not likely to present any difficulties due to the continuous nature of the new helipole geometry. The only restriction on the structure's use is that care must be taken to avoid striking the structure with the charged particle beam. The charging problem encountered can be alleviated however by positioning the electrode wires on the inside

surface of the insulating support tube.

REFERENCES

1. Septier,A. "Focusing of Charged Particles" Academic Press Inc.,New York, 1967,Volumes 1 and 2.

2. Septier,A Strong Focusing Lenses. Advances in Electronics and Electron Physics, Vol. 14,1961,p.85-205.

3. Hawkes,P.W. "Quadrupoles in Electron Lens Design". Advances in Electronics and Electron Physics, Supplement 7,1970.

4. Youssef,E.A. , Vermeulen,F.E. , Chute,F.S. A Note on Particle Trajectories in a Helical Electrostatic Quadrupole. Nuclear Instruments and Methods,93,1971,p.181-186.

5. Youssef,E.A. , Chute,F.S. , Vermeulen,F.E. Imaging Properties of a Novel Electrostatic Lens. Canadian Journal of Physics,49,2651,1971.

6. Vermeulen,F.E. , Youssef,E.A. , Chute,F.S. Experimental Investigation of the Imaging Properties of a Novel Electrostatic Lens. Canadian Journal of Physics,Vol.52, Number 5,1974,p.379-386.

7. Chute,F.S. , Vermeulen,F.E. , Youssef,E.A. , A Twisted Electrostatic Quadrupole for Guiding Heavy Charged Particles. Nuclear Instruments and Methods, 82,1970,p.86-92.

8. Kennedy,P.A. Electrolytic Tank, Design and Applications. Review of Scientific Instruments,Vol.27, Number 11,November 1956, p.916-927.

9. Spangenberg,K. "Vacuum Tubes" McGraw-Hill Bock Company, 1948,p.444

10. Goud,P.A. — Design Study of Accelerator Electron Guns. M.Sc. Thesis, Univ. of British Columbia,1961.

11. Moss,H. — "Narrow Angle Electron Guns and Cathode Ray Tubes", Acedemic Press, New York,p.145-150.

12. Youssef,E.A. — A Uniformly Twisted Electrostatic Quadrupole for Guiding and Imaging Charged Particles. Ph.D. Thesis, Univ.of Alberta,1973.

13. Heck,I.C. — "Magnetic Materials and Their Applications", Butterworth Company Ltd., London, 1974.

14. Patton,E.J. , Finch,J. — Design of a Room Size Magnetic Shield. Journal of Geophysical Research,Vol.67, Number 3,March 1962,p. 1117.

15, Wadey,W.G. — Magnetic Shielding with Multiple Cylindrical Shells. Review of Scientific Instruments, Vol.27, Number 11,Nov.1956, p.910-916.

16. Smythe — "Static and Dynamic Electricity" 3rd. Edition,McGraw-Hill Book Company Ltd., 1968,p.68-70.

17. Ramo,S. , Whinnery,J. , Van Duzer,T. — "Fields and Waves in Communication Electronics" John Wiley and Sons Inc., 1967, p.204.

18. Hayt,W.H. — "Engineering Electromagnetics" McGraw-Hill Book Company Ltd. 1967, p.86-92.

19. Jackson,J.D. — "Classical Electrodynamics" John Wiley and Sons Ltd., 1962, p.26-40,162-164.

20. Hepburn,J.D. — Generation and Acceleration of Charged Liquid Particle Beams. Ph.D. Thesis,University of Alberta, 1973.

APPENDIX A Scaling Factor

Once equation 2.4 is solved for the values of equivalent line charge density, equation 2.2 can be used to compute the potential at any point in the cross sectional (X,Y) plane of the new structure. In order to compare the computed (by 2.2) potential distribution Vc to the desired distribution $Vd=k(X^2-Y^2)$, one can pick some nominally arbitrary points in the plane and examine the error. Error is defined as $((Vd-Vc)/Vd)*100$, which gives one a percentage term. Since there is symmetry about both the X and the Y axis in both the number of wires and in the desired potential distribution, it is sufficient to examine only the first quadrant of the entrance plane. The error for a number of points in the first quadrant was calculated with the scaling factor D=1. The results are shown in Figure 25.

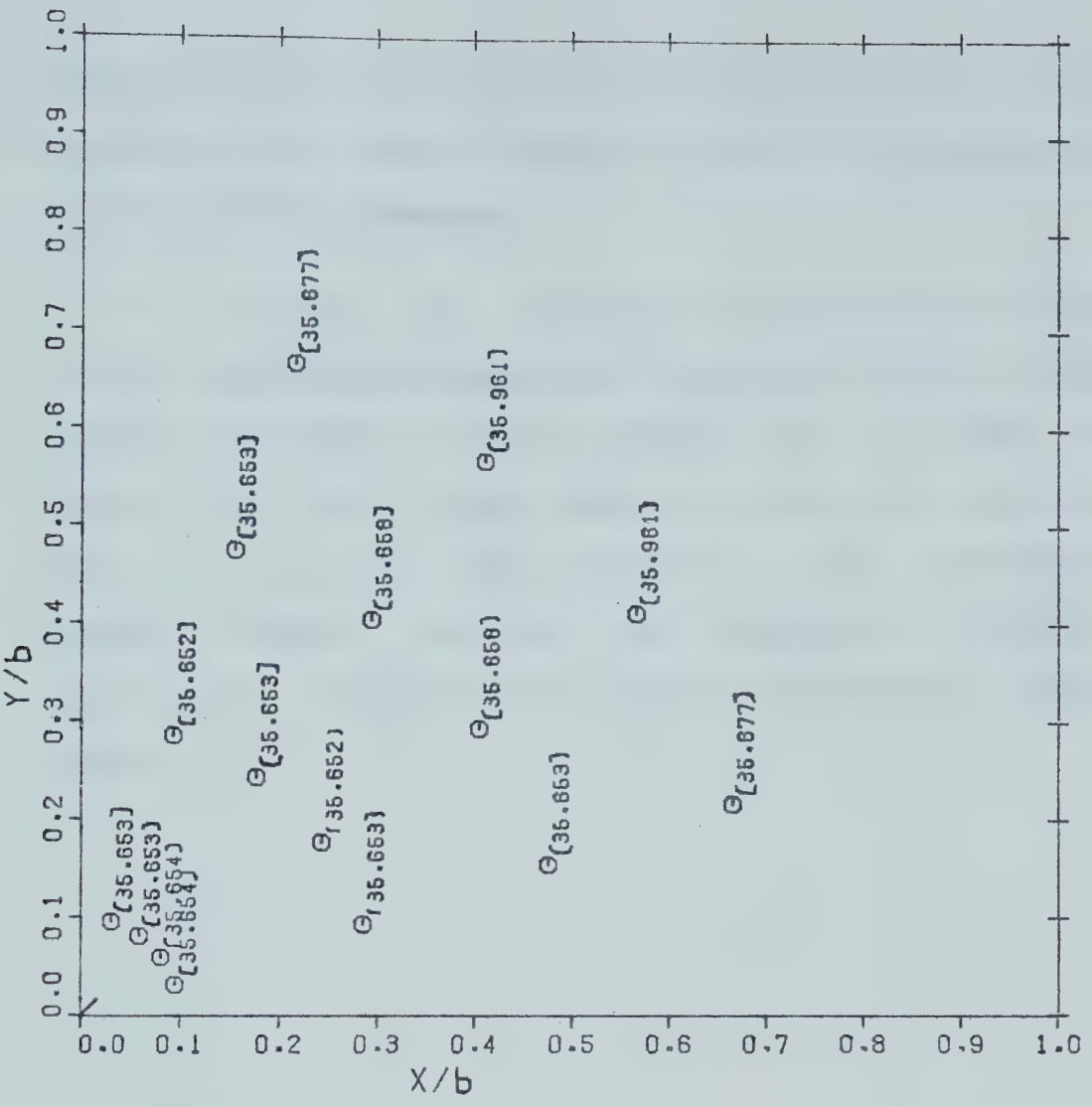

Figure 25: Error Distribution for a Scaling Factor of One

Obviously the calculated potential distibution does not compare well in amplitude with the desired distribution. However one will notice that the percentage error is almost constant for all points,

indicating that the calculated distribution varies with position in the desired manner but lacks the strength of the desired distribution.

If, however, an appropriate scaling factor (1.55 for the experimental structure's geometry) is put on the applied potentials, then the results are as shown in Figure 26. This figure shows that over the region of interest, i.e. the area enclosed by the dielectric support sleeve ($r<.76b$), the calculated potential distribution follows the desired distribution quite closely.

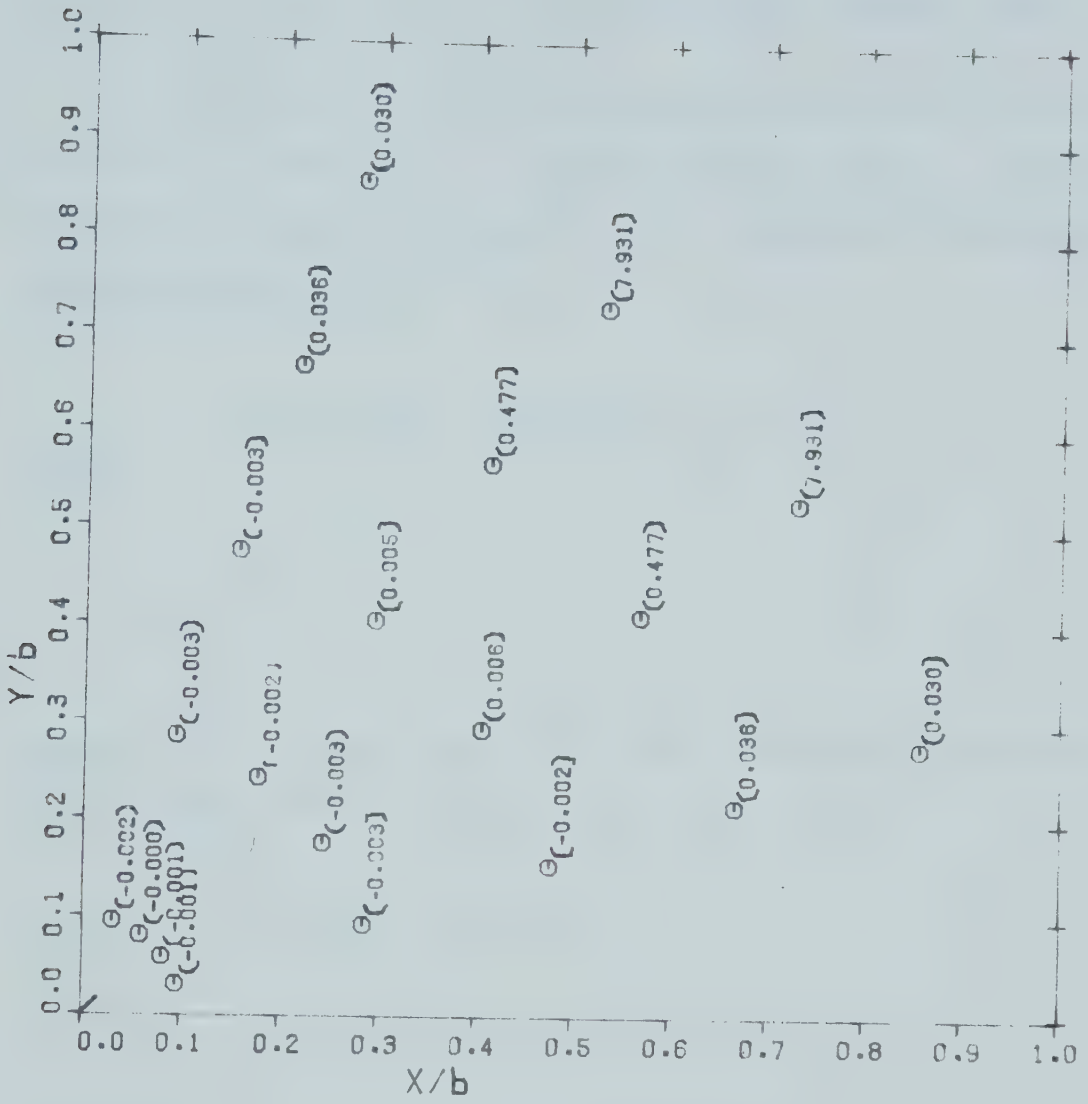

Figure 26: Error Distribution for a Scaling Factor of 1.55

APPENDIX B

Correction Factor Due to the Dielectric Support Tube

A solution for the boundary value problem shown in Figure 20 is sought. It can be shown[17] that a general solution to Laplace's equation for the desired potential distribution is

$$V_1(r,\phi) = (B_1 r^n + B_2 r^{-n})(B_3 \cos n\phi + B_4 \sin n\phi)$$

(B.1)

$$V_2(r,\phi) = (C_1 r^n + C_2 r^{-n})(C_3 \cos n\phi + C_4 \sin n\phi)$$

where the B's and C's are arbitary constants. Application of the boundary condition at r=b

(B.2)
$$V_2(r,\phi)\Big|_{\substack{r=b \\ \forall\phi}} = V_o \cos 2\phi$$

$$(C_1 b^n + C_2 b^{-n})(C_3 \cos n\phi + C_4 \sin n\phi) = V_o \cos 2\phi$$

implies

(B.3)
$$n = 2 \qquad C_4 = 0$$

and therefore

(B.4) $$(C_1 b^2 + C_2 b^{-2}) \cos 2\phi = V_o \cos 2\phi$$

where C_3 has been absorbed into C_1 and C_2,

from which one obtains

(B.5) $$V_2(r,\phi) = \left[C_1 r^2 + \frac{b^2(V_o - C_1 b^2)}{r^2}\right] \cos 2\phi$$

If one next applies the boundary condition at r=0

(B.6) $$V_1(r,\phi)\Big|_{r=0} < \infty$$

$$(B_1 r^2 + B_2 r^{-2})(B_3 \cos 2\phi + B_4 \sin 2\phi)\Big|_{r=0} < \infty$$

this implies

(B.7) $$B_2 = 0$$

and therfore

(B.8) $$V_1(r,\phi) = r^2(B_3 \cos 2\phi + B_4 \sin 2\phi)$$

There are two further boundary conditions at r=d

which are that the tangential electric fields must be equal and that the normal electric displacement densities must be equal i.e.

(B.9)
$$E_{tan1} = E_{tan2}$$
$$D_{n1} = D_{n2}$$

Applying the first of these boundary conditions

(B.10)
$$\left.\frac{1}{r}\frac{\partial V_1}{\partial \phi}\right|_{\substack{r=d \\ \forall \phi}} = \left.\frac{1}{r}\frac{\partial V_2}{\partial \phi}\right|_{\substack{r=d \\ \forall \phi}}$$
$$\left.2r(B_4 \cos 2\phi - B_3 \sin 2\phi)\right|_{\substack{r=d \\ \forall \phi}} = \left.-\frac{2}{r}\left(C_1 r^2 + \frac{b^2(V_o - C_1 b^2)}{r^2}\right)\sin 2\phi\right|_{\substack{r=d \\ \forall \phi}}$$

implies
$$B_4 = 0$$
(B.11)

from which

(B.12)
$$B_3 = C_1 + \frac{b^2(V_o - C_1 b^2)}{d^4}$$

Then applying the second boundary condition at r=d

(B.13) $$\left.\frac{\partial V_1}{\partial r}\right|_{r=d} = \varepsilon_r \left.\frac{\partial V_2}{\partial r}\right|_{r=d}$$

$$\left. 2r B_3 \cos 2\phi \right|_{r=d} = \varepsilon_r \left(2C_1 r - \frac{2b^2(V_0 - C_1 b^2)}{r^3} \right) \cos 2\phi \Big|_{r=d}$$

from which

(B.14) $$B_3 = \varepsilon_r \left(C_1 - \frac{b^2(V_0 - C_1 b^2)}{d^4} \right)$$

Combining equation B.12 and B.14 yields:

(B.15) $$B_3 = \frac{b^2 V_0}{d^4} \left[\frac{\left(\frac{\varepsilon_r + 1}{\varepsilon_r - 1}\right)\left(1 - \frac{b^4}{d^4}\right)}{1 + \left(\frac{\varepsilon_r + 1}{\varepsilon_r - 1}\right)\frac{b^4}{d^4}} + 1 \right]$$

Finally substituting B_3 and $B_4 = 0$ into equation B.8 gives one

$$V_1(r, \phi) = K_1 \frac{V_0}{b^2} r^2 \cos 2\phi$$

(B.16) $$K_1 = \frac{b^4}{d^4} \left[\frac{\left(\frac{\varepsilon_r + 1}{\varepsilon_r - 1}\right)\left(1 - \frac{b^4}{d^4}\right)}{1 + \left(\frac{\varepsilon_r + 1}{\varepsilon_r - 1}\right)\frac{b^4}{d^4}} + 1 \right]$$

which is the potential distribution in the free space

region inside of the dielectric sleeve.